SOLAR SHIFT: A PERSPECTIVE ON BUILDING ENERGY PERFORMANCE UNDER HAZE POLLUTIONS IN CHINA

A Thesis
Presented to
The Academic Faculty

By

Yiyuan Jia

In Partial Fulfillment
of the Requirements for the Degree
Master of Science in the
School of ARCHITECTURE

Georgia Institute of Technology
August 2016

SOLAR SHIFT: A PERSPECTIVE ON BUILDING ENERGY PERFORMANCE UNDER HAZE POLLUTIONS IN CHINA

Approved by:

Prof. Godfried Augenbroe, Advisor
School of Architecture
Georgia Institute of Technology

Dr. Jason Brown
School of Architecture
Georgia Institute of Technology

Dr. Nadir Abdessemed
Transsolar Inc.

Date Approved: May 18th, 2016

To a brighter and cleaner future

ACKNOWLEDGEMENTS

I wish to thank people along the way who has supported and inspired me in pursuing this study.

First and foremost, I would like to thank my advisor Prof. Godfried Augenbroe for his guidance, support and offering me great freedoms in choosing this thesis project.

I want to thank my thesis committee member Prof. Jason Brown and Dr. Nadir Abdessemed for their careful examinations and invaluable suggestions to improve this work. I want to thank Dr. Christian A. Gueymard, Dr. Joe Huang and Dr. Xiangao Xia for their guidance and patience in responding the endless emails from me and for sharing their insights and knowledge about this study without any reservations.

I would like to extend my sincere thanks to my mentors during my internships at Transsolar KlimateEngineering, Erik Olsen and Linda Lam. Erik has first pointed out that the haze pollution could have a potential impact on solar budget during a project discussion, which has triggered this study. Linda has shown great support in helping me targeting a thesis topic.

Lastly, I want to thank the PIs in the AERONET and OpenEI projects for their establishment and maintenance of the datasets and making them open sources to the public. Many thanks to Prof. Peng Xu and his group at Tongji University for creating and sharing the Chinese reference building models which has been adopted in this study.

The creation of this thesis is associated with approximately 4.7 tons of CO_2 Equivalents.

TABLE OF CONTENTS

LIST OF TABLES

LIST OF FIGURES

LIST OF SYMBOLS AND ABBREVIATIONS

BEM	Building Energy Modeling
ASHRAE	American Society of Heating, Refrigerating, and Air-Conditioning Engineers
AOD	Aerosol Optical Depth
BAOD	Broadband Aerosol Optical Depth
PM2.5	Airborne Fine Particles Less Than 2.5 Microns in Diameter
TMY	Typical Meteorological Year
AMY	Actual Meteorological Year
GDP	Gross Domestic Product
DRF	Aerosol Direct Radiative Forcing
TOA	Top of Atmosphere
CSWD	Chinese Standard Weather Data
CTYW	Chinese Typical Year Weather
SWERA	Solar and Wind Energy Resource Assessment
DOY	Day of Year
DNI	Direct Normal Irradiance
GHI	Method for Global Horizontal Irradiance
DIF	Diffuse Horizontal Irradiance
AERONET	Aerosol Robotic Network
NREL	National Renewable Energy Laboratory
EUI	Energy Use Intensity
CDF	Cumulative Distribution Function
SHGC	Solar Heat Gain Coefficient
METSTAT	Meteorological/Statistical Solar Radiation Model

SUMMARY

The severe haze pollution in China has arisen concerns among the public and government officials, due to its impacts on pubic health, visibility, climate and agriculture. To augment these findings of the negative impacts of haze pollution, this study investigates the "solar shift" effect due to haze pollutions and the potential (unreported) impacts on buildings' energy performance in China.

In a severe haze event, the suspended aerosol particles absorb and scatter solar beams such that the solar irradiance reaching to the building's envelope are truncated and redistributed. The altered solar budget affects building's heating and cooling load profiles and further impacts the heating and cooling energy consumptions.

In this study, we take the aerosol optical depth (AOD) as a measure of the solar blocking effect of haze pollutions. By plugging in the measured and projected AOD data in solar models, we develop three weather files for Beijing that represent different haze pollution for the following scenarios: the 2014 situation, the optimistic projection of 2050 (2050A) and the pessimistic projection of 2050 (2050B). Together with the TMY (Wilcox and Marion 2008, https://energyplus.net/weather/sources#SWERA), these weather files serve as the boundary conditions in building energy modeling practices. The results indicate the district heating energy consumption under the 2014 aerosol emission levels would increase 5 % compared to the current practice using TMY weather file. In the pessimistic scenario where we assume to keep the current pace of aerosol emissions, the district heating energy would increase 10 %. The current ASHRAE design day sizing method would assure the heating load being met under all possible scenarios investigated in this study.

CHAPTER 1

INTRODUCTION

1.1 Background

Haze pollution in China has drawn great attentions in recent years. On December 8th 2015, the Chinese government for the first time ever declared a red alert (under the four-tier alert system) in Beijing due to measured and expected high pollution levels. Vehicles were limited on roads, schools were closed, all construction sites were halted and citizens were suggested to stay indoors (BBC News 2015).

Since 2008, the U.S. embassy in Beijing started to monitor the ambient air and measured the hourly concentration of the airborne fine particles less than 2.5 microns in diameter (PM2.5) for their own purpose. The real-time measurement data then spread through the social media and later have created a focus and discussions among a wider group of people including both the public and government officials.

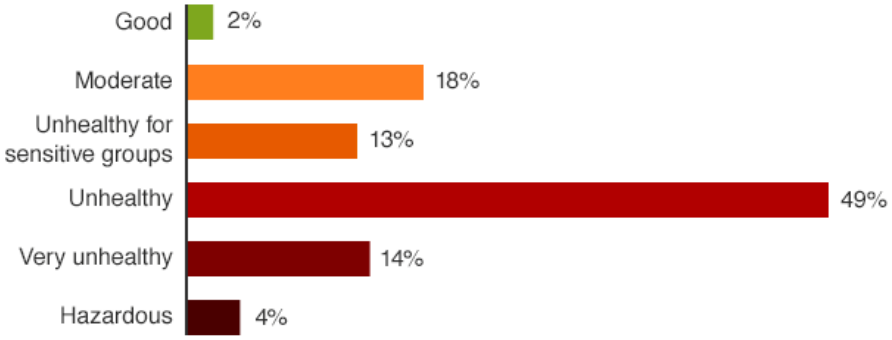

Figure 1. Daily average air quality index (AQI) at US embassy Beijing, based on PM2.5 concentration reading from 2008 to 2015. AQI categories as set by the US Environment Protection Agency (BBC News 2015)

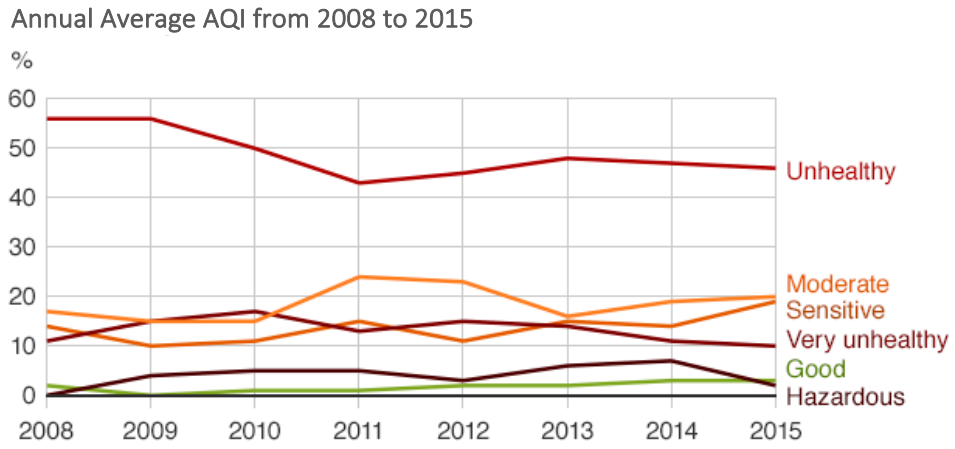

Figure 2. Annual average air quality index (AQI) at US embassy Beijing, based on PM2.5 concentration reading from 2008 to 2015 (BBC News 2015)

Haze is a combined effect of air pollution and local atmospheric conditions. When the horizontal visibility is equal to or less than 10 km and atmospheric relative humidity (RH) is equal to or less than 90 %, the atmospheric phenomenon is called haze (Wang, Wang et al. 2012). By nature, haze results from suspended fine aerosol particles (i.e. PM2.5) in the air. The sources of these fine particles are mainly industrial emissions, vehicle exhaust pollutants and secondary aerosol formed through a series of photochemical reactions (Liu, Li et al. 2013).

China has experienced a rapid economic growth since the 1980s, this dramatic growth has also led to severe air pollution in the major cities across of the country. In one of the most severe and persistent haze episode during the first quarter of 2013, around 1.3 million km^2 and 800 million people were affected. The daily average PM2.5 measurement of 74 major cities reaches 75 ug/m^3 (about twice of the US EPA standard of 35 ug/m^3) for 69% of the days on January, with a record-breaking daily concentration of 772 ug/m^3 (Huang, Zhang et al. 2014).

Figure 3. The “airprocalypse” scenery of Beijing on December 2015 when declared its first ever red alert for severe air pollution (BBC News 2015)

Figure 4. The same view when the haze is gone (BBC News 2015)

There are four major areas in China suffering from severe haze pollution: The Jing-Jin-Ji Region, the Yangtze River Delta, the Pearl River Delta (PRD) and the Sichuan Basin. The regional variation of pollution shows that northern China is more severe than southern China(Yang, Liu et al. 2015). This can be attributed to the central hearing systems of northern China, which extract heating energy from burning fossil fuels (coals mainly) in a centralized boiler station and supply heat to multiple buildings in a community. The strategy is largely implemented in the residential building sector of northern China. In addition, the lower rainfall of the northern regions also strengthens the haze pollution.

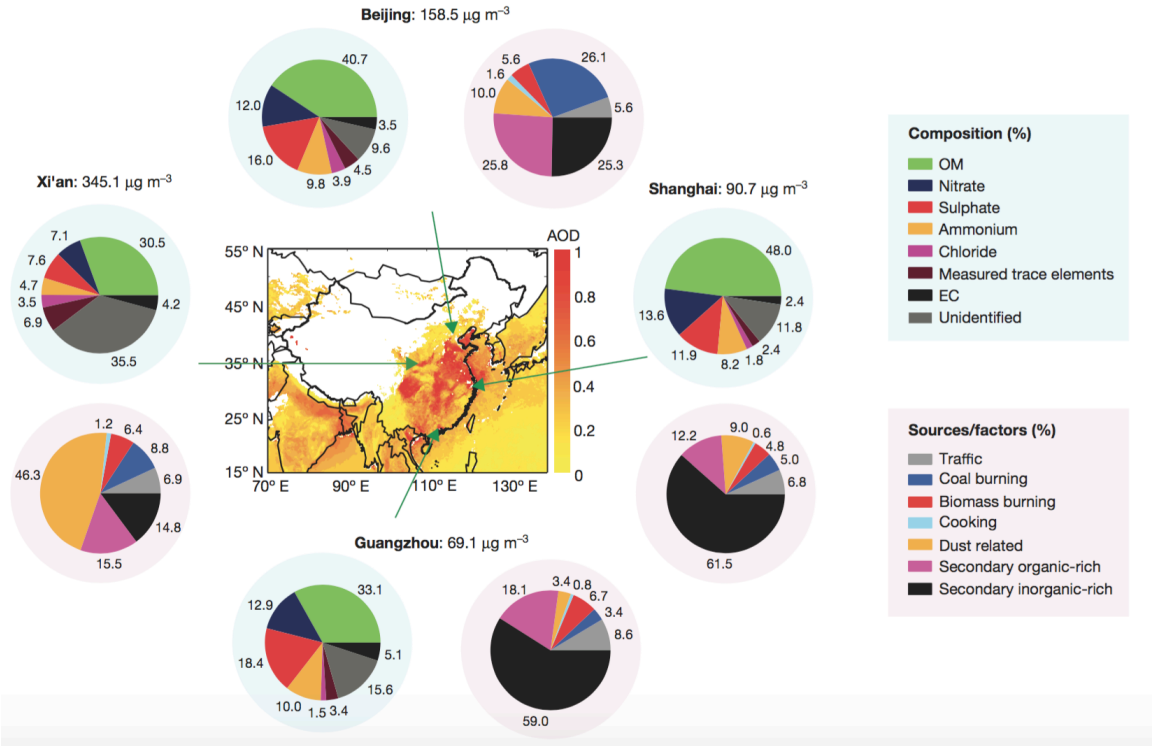

Figure 5. Composition and source of PM2.5 during the high pollution event on Jan. 2013 at Major Chinese cities (Huang, Zhang et al. 2014)

1.2 Aerosols and Direct Radiative Forcing

Atmospheric aerosols play an important role in global and regional climate change through modification of solar radiation budget. Aerosols directly absorb and scatter solar radiation and truncate the amount of solar irradiance reach to the earth's surface. Indirectly, aerosols modulate cloud properties and abundance (Stier, Seinfeld et al. 2007).

Atmospheric aerosols could be attributed to two sources, the natural and anthropogenic activities. Most of the natural aerosols are from mineral dust and marine aerosols. Anthropogenic aerosols are primarily emitted from burning of biomass and industrial pollutions, although some biomass-burning emissions are due to naturally occurring large-scale fires in tropical and boreal regions (Bellouin, Boucher et al. 2005).

The aerosol direct radiative forcing (DRF) is defined as the perturbation of the radiative fluxes caused by anthropogenic aerosols (natural aerosols are not included) (Bellouin, Boucher et al. 2005). DRF is normally studied at the top of the atmosphere (TOA) as well as at the surface of the ground. Given our study objects are buildings, we are interested in the DRF at ground surface. (Liu, Xia et al. 2007) has examined the aerosol direct forcing effect during an severe pollution episode occurred at October 2014 in Northern China, the results have shown that the variation of aerosol optical depth (AOD) levels, the reflected irradiance at the TOA and the ground surface irradiance change dramatically. The study also mentioned at the peak of the pollution episode, when the AOD at 500 nm is reaching to 4 (an unitless scale of AOD), the instant reflected irradiance at the TOA increases by 50 W/m^2, and the instant surface irradiance has decreases by 350 W/m^2.

1.3 Building Energy Modeling and Weather data

Building energy modeling (BEM) is a practical and well-established methodology in assessing building's energy performance. The basic approach of BEM is to apply physical principle based models of heat and mass flow around buildings to predict operational energy use intensity (EUI), as summarized by Reinhart and Davila (Reinhart and Davila 2016). Over the last few decades, building energy simulation has significantly matured and a broad range of BEM toolkits have become available, such as EnergyPlus, eQuest, TRNSYS (Laboratory and Klein 1979, Crawley, Lawrie et al. 2001, Hirsch 2006).

BEM is a recognized and indispensable practice that has a place in different stages of a project. Applications of BEM include (but are not limited to) design decision analysis, equipment sizing, life cycle cost analysis, building energy auditing, retrofit and commissioning. In this study, we use BEM to simulate the environmental impacts on the EUI, the latter is assumed to be a good measure of the actual energy use intensity in an actualized building.

Weather is one of the important driving forces of building behaviors. In BEM practices, the varying weather phenomena is represented in the form of short interval data, i.e. monitored or modeled hourly values. These data provide boundary conditions for the component models that are combined in simulation applications (Barnaby and Crawley 2011). The most commonly used weather data format is Typical Meteorological Year (TMY). TMY file contains a full year (8760 hours) of weather data that are needed for building simulation, which are not necessarily from the same year, rather they are composite of weather data for each typical months.

Table 1. Weather data items of use for building simulations (Barnaby and Crawley 2011)

Item	*Model use(s)*	*Availability and issues*
Dry-bulb air temperature	• Exterior surface convection • Infiltration/ventilation sensible heat transfer • Equipment (e.g. air-cooled condenser)	• Universally observed • Significant local effects (e.g. heat island)
Humidity (one of relative humidity, wet-bulb temperature, or dew-point temperature)	• Infiltration/ventilation latent heat transfer • Equipment (e.g. cooling tower)	• Commonly observed
Solar irradiance (direct and diffuse)	• Fenestration heat gain • Exterior surface heat balance • Solar thermal and photovoltaic systems	• Sparsely measured • If observed, often global only • Model sources widely used • Remote sensing opportunities
Solar illuminance (direct and diffuse)	• Daylight modeling	• Rarely measured (modeled from irradiance)
Sky temperature	• Exterior surface heat balance	• Rarely measured (modeled from temperature, humidity, and cloud cover)
Cloud cover/sky condition	• Sky models (e.g. for daylighting)	• Generally observed • Multiple data representation conventions • Evolution of automated instrumentation introduces uncertainties
Wind (velocity and direction)	• Exterior surface convection • Infiltration • Natural ventilation	• Generally observed • Local effects very significant for both velocity and direction • Low velocity observations unreliable
Ground temperature	Below-grade heat transfer	• Measured for agricultural purposes, limited exploitation of observed values for building simulation
Ground surface albedo	Reflected irradiance/illuminance	• Inferred from presence of snow
Weather conditions (e.g. rain)	Exterior surface wetting	• Generally measured; inconsistent reporting formats

Table 1 shows common weather data items that have applications on building simulation. Solar irradiance (direct and diffuse components) are essential in the heat balance equations that represents the physical behavior around fenestration, interior and

exterior surfaces. In addition, it should also be noted that, solar illuminance is a direct driver of daylight simulation, although it is not a major focus in this study.

A critical issue to keep in mind is that solar data used in building simulation are sparsely measured. With few exceptions, solar irradiance and illuminance in current TMY weather files are modeled. It is reported that in TMY3 data set, less than 40 among 1020 sites include measured solar data (Barnaby and Crawley 2011).

There are three versions of Chinese weather files available at the EnergyPlus website (https://energyplus.net/weather/sources). Below are recorded descriptions of the weather files:

Chinese Standard Weather Data (CSWD)

"Developed for use in simulating building heating and air conditioning loads and energy use, and for calculating renewable energy utilization, this set of 270 typical hourly data weather files. These data were developed by Dr. Jiang Yi, Department of Building Science and Technology at Tsinghua University and China Meteorological Bureau. The source data include annual design data, typical year data, and extreme years for maximum enthalpy, and maximum and minimum temperature and solar radiation."

Chinese Typical Year Weather (CTYW)

"Developed for use in simulating building heating and air conditioning loads and energy use, and for calculating renewable energy utilization, this set of 57 weather files is based on a 1982-1997 period of record with data obtained from the U. S. National Climatic Data Center. The original data set was created by Prof. ZHANG Qingyuan of Tsukuba University Japan, in collaboration with Joe Huang of Lawrence Berkeley National Laboratory."

Solar and Wind Energy Resource Assessment (SWERA)

"The Solar and Wind Energy Resource Assessment (SWERA) project, funded by the United Nations Environment Program, is developing high quality information on solar and wind energy resources in 14 developing countries. Typical year hourly data are

available for 156 locations in Belize, Brazil, China, Cuba, El Salvador, Ethiopia, Ghana, Guatemala, Honduras, Kenya, Maldives, Nicaragua, and Sri Lanka."

1.4 Motivation

Many studies have reported the negative impacts of haze pollution on visibility, public health, local and global climate and agriculture (Chameides, Yu et al. 1999, Fu, Zhuang et al. 2008, Kan, Chen et al. 2012, Chen, Wang et al. 2013). Buildings, as an interface connecting people and the outdoor environment, are both actively and passively responsive to the changes of boundary conditions due to ambient climate conditions. Despite these facts, buildings have not been studied in the presence of haze pollutions.

As the haze pollution in China has been shown to have impacts on occupants and climate, one would naturally extend a question as how would the haze pollution impact a building's operational behavior.

In 2010, building account for more than 20% of China's total energy consumption (Hong, Yang et al. 2014), the total national building energy consumption (TNBEC) is around 16 billion tons standard coal. This number is projected to increase as a consequence of the continued economic growth, rapid urbanization and people's demand for better living standard. Building energy consumption in China would be of primary interest if haze pollution were to have a significant influence on building energy use.

1.5 Research Questions and Hypothesis

Intuitively, haze pollutions would have causal effects on building energy consumptions from the following perspectives:

1. Solar heat gain posed on the exterior of a building is reduced due to increased aerosol levels.
2. Reducing daylight availability leads to increased artificial lighting consumption.

3. The relative humidity of outdoor air that strengthened by the haze pollution could have influence on HVAC operational efficiency.
4. Natural ventilation availability is reduced.
5. More pressure drop due to the necessity of high grade filters, leading increased fan energy consumption.
6. Occupancy schedules could be affected by severe outdoor environment.
7. Increased appliance load (air purification equipment).

Among these potential causes, solar radiation has a direct and potentially significant influence on building energy consumption. The sun strikes energy on building's envelope through radiative heat transfer. These heat gains are then added to the air sensible heating/cooling demand through conductive and convective heating transfer. The sensible heating/cooling demand leads to energy consumptions by the heating or cooling systems that operate to meet the thermal demand. In winter, solar heat gain provides "free heating" thus potentially reducing heating energy consumption. In summer, solar heat gains pose more cooling demand leading to more energy consumption by the cooling system. The direct radiative forcing effect caused by the increased aerosol levels would lead to a variation in building energy consumption.

This thesis develops and tests the following hypothesis:

- *Hypothesis 1*: The variation of daily aerosol emission levels will impact China's daily solar radiation budget in the long term.
- *Hypothesis 2*: The projected variations of solar radiation budget will further impact buildings' heating and cooling energy consumption patterns.
- *Hypothesis 3*: The future change of heating energy consumption pattern due to aerosol emission levels in time cause the HVAC system, sized under the current climate, to be inadequate to the future heating load under a rising aerosol emission rate.

To test the first hypothesis, two future AOD profiles are generated based on optimistic and pessimistic projections based on the measured 2014 AOD level in Beijing, China. We adopt a clear sky solar radiation model that takes aerosol parameters (AOD) as the major input, the model will calculate the solar irradiance components (GHI, DNI, DIF) under clear sky conditions. The cloud information is extracted from the TMY weather file and can be represented by a cloud factor. The future solar radiation profiles are generated through modifying the model-calculated clear sky irradiances and the TMY cloud factor.

To test the second hypothesis, we generate new sets of weather files by taking the TMY file as the base and replacing the solar irradiances with the future solar radiation profiles which are derived by the proposed methodology. A Chinese reference building is used as the object of several case studies. The energy consumptions are simulated in the building model by plugging in the weather files that represents different projections of the aerosol emission levels.

To test the third hypothesis, we estimate the "ideal sensible heating load" by simulating a revised building model without the mechanical heating and cooling systems. The load profiles are generated for all weather scenarios and plotted as cumulative probability distribution curves. The 99.6 percentiles of each scenario is compared with the sizing result through the ASHRAE design day method.

1.6 Thesis Outline

This thesis develops as the following order: Chapter 1 introduces general background information on the haze pollution situation in China and the motivation of the study. Chapter 2 describes the solar radiation modeling methodology adopted in this study, the clear sky solar radiation modeling methods are further validated with the TMY weather file. Chapter 3 creates the future projection of AOD profiles based on literature review and further proposes a methodology to create new weather files based on the

methods introduces in Chapter 2. Chapter 4 provides case studies of building energy consumptions that utilize the weather files generated in Chapter 3 and a reference building energy model. Chapter 5 concludes the findings and projects the future work.

CHAPTER 2

SOLAR RADIATION MODELING

2.1 The Solar and Wind Energy Resource Assessment Project

The Solar and Wind Energy Resource Assessment (SWERA) is an initiative among multiple international organizations that creates a user-oriented environment for solar and wind recourse data sharing and analysis. The targeted user group of the data set are policymakers, project planners, research analyst and investors.

The SWERA project started in 2001 with the ambition to scale up and advance the renewable energy technologies by providing high quality solar and wind resources data over the world. Thirteen pilot countries are involved in the project: Bangladesh, Brazil, China, Cuba, El Salvador, Ethiopia, Ghana, Guatemala, Honduras, Kenya, Nepal, Nicaragua and Sri Lanka.

The SWERA project was funded by the Global Environment Facility (GEF) and managed by United Nations Environment Program's Division of Technology. Some of the contributors include (http://en.openei.org/wiki/SWERA/About):

- National Renewable Energy Laboratory (NREL)
- German Aerospace Center (DLR)
- Risoe National Laboratory for Sustainable Energy
- Brazil's National Institute for Space Research (INPE)
- State University of New York (SUNY)
- United Nations Environment Programme (UNEP)
- National Aeronautics and Space Administration
- Global Environment Facility (GEF)
- Risoe DTU

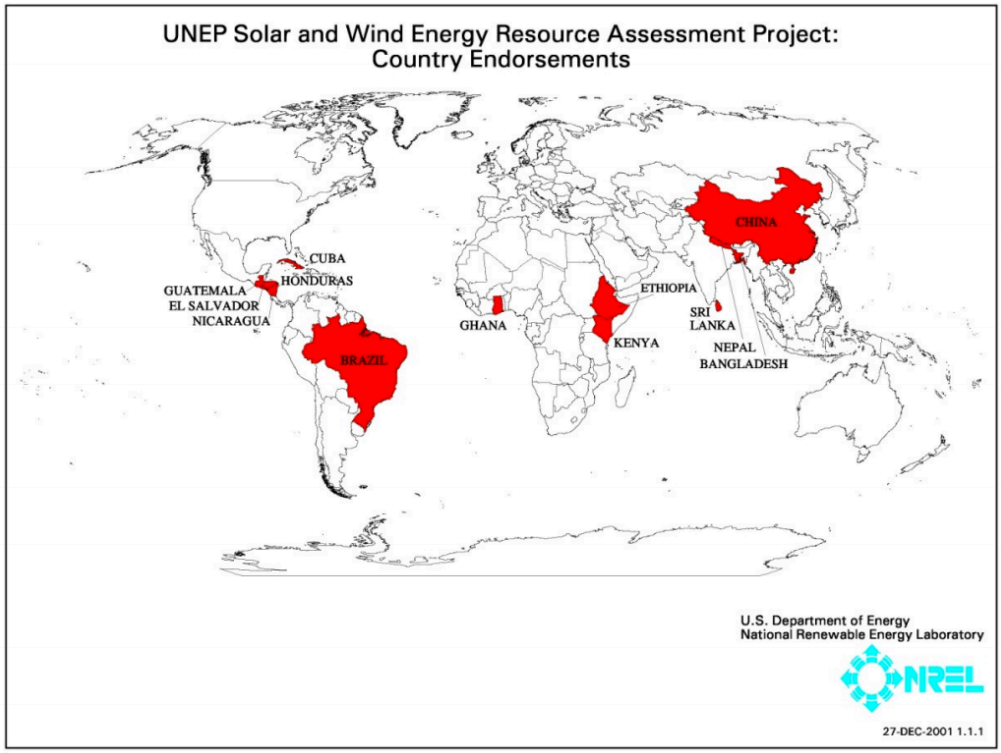

Figure 6. The thirteen pilot countries selected in the SWERA initiative (The User Manual for SWERA 2006)

The SWERA project provide multiple hourly data sets (Solar, Wind, TMY, etc.) and toolkits for data analysis and visualization for certain stations in select countries. The original intended use of the solar radiation data was to perform computer simulation and evaluation of solar energy conversion systems and building systems. The SWERA TMY datasets include 8760 hours of direct normal irradiance (DNI), global horizontal irradiance (GHI) and diffuse horizontal irradiance (DIF) and other climatic parameters. The SWERA TMY file for Beijing downloaded from the EnergyPlus website is among these available data sets, it is generated based on the Actual Meteorological Year (AMY) data from 1973 – 2002. These AMY data are available at the OpenEI website (http://en.openei.org/wiki/Main_Page).

Given the nature of SWERA project, the solar radiation data in the SWERA TMY file could be trusted in solar related energy calculations. With that, we take the SWERA TMY data for Beijing as our reference weather file.

2.2 Clear-Sky Models

As mentioned in previous section, the majority solar irradiance data in the existing TMY files are modeled rather than measured. In general, two layer of models are adopted in the modeling procedures. The first layer is a clear-sky irradiance model, which calculates the solar irradiance under cloudless sky conditions. The second layer is a cloud model. It takes ground observed or satellite derived cloud information to derive a "cloud modifier". The clear-sky irradiance will be further modified by the "cloud modifier" to generate the solar irradiance under cloudy conditions.

Many clear-sky irradiance models can be found in literature (Bird and Hulstrom 1981, Ineichen 2008, Lefevre, Oumbe et al. 2013).18 clear-sky irradiance models are compared by Gueymard in (Gueymard 2012) in term of computational algorithms and model performance. One of the major difference among the 18 models is their algorithm in calculating the aerosol transmittance, section 2.4 describes several algorithms in modeling aerosol transmittance from different clear sky models. Five models (REST1, Ineichen, Hoyt, Bird, and Iqbal-C) are reported to have constantly high rankings in predicting direct irradiance. (Sengupta and Gotseff 2013) evaluated Bird, SolisBB and REST2 models and concluded that the Bird model has an overall good balance between computation speed as well as model performance.

The solar position and extraterrestrial radiation features are common among different clear-sky models, which are described below.

Solar Position

The intensity of solar energy that reaches the earth surface is highly dependent on the relative geometry of the sun and receiver on the ground surface. Thus all clear sky models require geometric inputs describing the solar zenith angle throughout the year. At solar noon on either the spring or fall equinox, the zenith angle (z) is equal to the latitude of the site (ϕ):

$$z = \phi \tag{2.1}$$

During any other day of the year (DOY), the zenith angle at solar noon is calculated by subtracting the declination angle (δ):

$$z = \phi - \delta \tag{2.2}$$

Declination angle is calculated using a Fourier series equation:

$$\delta = 0.006918 - 0.399912 \cdot \cos(xx) + 0.07257 \cdot \sin(xx) - 0.006758 \cdot \cos(2xx) + 0.000907 \cdot \sin(2xx) - 0.006758 \cdot \cos(3xx) + 0.00907 \cdot \sin(3xx) \tag{2.3}$$

Where,

$$xx = \frac{2\pi}{365}(DOY - 1) \tag{2.4}$$

The solar time is calculated based on the difference between a site's longitude and the meridian of its time zone, and the yearly perturbations in the earth's rate of rotation around the sun:

$$Solar\ Time = Local\ Time + (Standard\ Meridan - Local\ Meridan) \cdot 4 + EOT$$

Where

$$EOT[min] = 9.87 \cdot \sin(2x) - 7.53 \cdot \cos(2x) - 1.5 \cdot \sin(x) \tag{2.5}$$

With

$$x = \frac{2\pi}{365}(DOY - 81) \tag{2.6}$$

The hour angle (ω) is the angle between the line pointing directly to the sun and the line pointing directly to the sun at solar noon. Note that the hour angle is just an angular representation of solar time, and fifteen degrees represent one hour:

$$w[deg] = (Solar\ Time[h] - 12) \cdot 15 \tag{2.7}$$

The true zenith angle for any date, time, and location can be calculated using the declination angle, solar time, and site latitude:

$$\cos(z) = \cos(\phi)\cos(\delta)\cos(\omega) + \sin(\phi)\sin(\delta) \tag{2.8}$$

Extraterrestrial Radiation

The extraterrestrial radiation, or the radiation that reaches the outer part of earth's atmosphere, varies slightly throughout the year. To account for the eccentricity of the Earth's orbit around the sun, the extraterrestrial radiation is calculated with a yearly varying term.

$$I_0 = 1367.7 \cdot [1 + 0.033 \cdot \cos(\frac{2\pi}{365} \cdot DOY)] \quad (2.9)$$

$$I_0 = I_{SC} \cdot [1.00011 + 0.034221 \cdot \cos(\mathrm{x}) + 0.00128 \cdot \sin(\mathrm{x}) - 0.000719 \cdot \cos(2x) + 0.000077 \cdot \sin(2x)] \quad (2.10)$$

where,

$$I_{SC} = 1366.1\ W/m^2 \quad (2.11)$$

2.3 Solar Radiation Modeling in SWERA

Method for Direct Normal Irradiance (DNI)

The direct normal irradiance (DNI) calculation in SWERA project is based on the Bird clear sky model (Bird and Hulstrom 1981) and modified by coefficients representing cloudy conditions.

$$DNI = 0.9751 \cdot I_0 \cdot \tau_R \cdot \tau_{Gas} \cdot \tau_{WV} \cdot \tau_{Ae} \cdot \tau_{Ozone} \cdot \tau_{vis} \cdot \tau_{ir} \quad (2.12)$$

The atmospheric transmittance coefficients τ_i are calculated using atmospheric measurement data.

Transmittance for Rayleigh scattering

$$\tau_R = \exp[-0.0903 {am_p}^{0.84}(1.0 + am_p - {am_p}^{1.01})] \quad (2.13)$$

Transmittance for equally distributed gas (mainly O_2 and CO_2)

$$\tau_{Gas} = \exp(-0.0127 {am_p}^{0.26}) \quad (2.14)$$

Transmittance for Ozone

$$\tau_{Ozone} = 1 - \alpha_{Ozone} \tag{2.15}$$

$$\alpha_{Ozone} = 0.1611\chi(1.0 + 139.48\chi)^{-0.3035} - 0.002715\chi(1.0 + 0.044\chi + 0.003\chi^2)^{-1} \tag{2.16}$$

$\chi = u \cdot am$, with the vertical ozone layer thickness u in cm [NTP] and the air mass am.

Transmittance for water vapor

$$\tau_{WV} = 1 - \alpha_{WV} \tag{2.17}$$

$$\alpha_{WV} = 2.4959\gamma[(1.0 + 79.034\gamma)^{0.6828} + 6.385\gamma]^{-1} \tag{2.18}$$

$\gamma = w \cdot am$, with the pressure-correlated relative optical path length of perceptible water w in cm [NTP].

Transmittance for aerosols

$$\tau_{Ae} = \exp\left[-{k_a}^{0.873}(1.0 + k_a - {k_a}^{0.7088}){am_p}^{0.9108}\right] \tag{2.19}$$

$$k_a = 0.2758k_{a\lambda_{\lambda=0.38\mu m}} + 0.35k_{a\lambda_{\lambda=0.5\mu m}} \tag{2.20}$$

with the aerosol optical depth $k_{a\lambda_\lambda}$ at the wave length 0.38 μm and 0.5 μm.

Transmittance for clouds

Using the visible Cloud-Index Cl_{vis}

$$\tau_{vis} = e^{(-Cl_{vis}\cdot 0.1)} \tag{2.21}$$

And using the infrared Cloud-Index Cl_{ir}

$$\tau_{ir} = e^{(-Cl_{ir}\cdot 0.07)} \tag{2.22}$$

For clear-sky atmospheric transmittance, the air mass is needed which is calculated by

$$am = \frac{1}{[cos\Theta_Z + 0.15(93.885 - \Theta_Z)]^{-1.253}} \tag{2.23}$$

The pressure correlation is made by

$$am_p = am \cdot \frac{p}{1013.25} \tag{2.24}$$

Method for Global Horizontal Irradiance (GHI)

GHI in the DLR model is calculated based on the method developed by (Perez, Moore et al. 2002)

$$GHI = ktm \cdot Ghc \cdot (0.0001 \cdot ktm \cdot Ghc + 0.9) \tag{2.25}$$

where ktm is a cloud modifier, and Ghc is the clear-sky global horizontal irradiance.

$$ktm = 2.36 \cdot CI^5 - 6.2 \cdot CI^4 + 6.22 \cdot CI^3 - 2.63 \cdot CI^2 - 0.58 \cdot CI + 1 \tag{2.26}$$

$$Ghc = cg1 \cdot I_0 \cdot cos\Theta_Z \cdot \exp(-cg2 \cdot am \cdot (fh1 + fh2 \cdot (TL - 1))) \cdot \exp(0.01 \cdot am^{1.8}) \tag{2.27}$$

Where,

$$cg1 = (0.0000509 \cdot alt + 0.868) \tag{2.28}$$

$$cg2 = (0.0000392 \cdot alt + 0.0387) \tag{2.29}$$

$$fh1 = \exp\left(-\frac{alt}{8000}\right) \tag{2.30}$$

$$fh1 = \exp\left(-\frac{\text{alt}}{1250}\right) \tag{2.31}$$

The Linke turbidity is derived using the following formulation derived by (Perez, Ineichen et al. 2002)

$$TL = \frac{11.1 \cdot \ln\left(b \cdot \frac{I_0}{B_{ncl}}\right)}{am} + 1 \tag{2.32}$$

with

$$b = 0.664 + \left(\frac{0.163}{fh1}\right) \tag{2.33}$$

and the clear-sky direct normal irradiance

$$B_{ncl} = I_0 \cdot \tau_R \cdot \tau_{Gas} \cdot \tau_{WV} \cdot \tau_{Ae} \cdot \tau_{vis} \tag{2.34}$$

In order to be consistent with the DNI calculation, we used Bird's formulation in calculating Ghc (Bird and Hulstrom 1981)

$$Ghc = \frac{I_d + I_{as}}{1 - r_g \cdot r_s} \tag{2.35}$$

Where,

$$I_d = DNI \cdot cos\Theta_Z \tag{2.36}$$

$$I_{as} = 0.79 \cdot I_0 \cdot \tau_{Gas} \cdot \tau_{WV} \cdot \tau_{AA} \cdot \tau_{Ozone} \cdot cos\Theta_Z \cdot \frac{[0.5 \cdot (1 - \tau_R) + B_a \cdot (1 - \tau_{AS})]}{[1.0 - am + am^{1.02}]} \tag{2.37}$$

$$\tau_{AA} = 1 - K_1 \cdot (1.0 - am + am^{1.06}) \cdot (1 - \tau_{Ae}) \tag{2.38}$$

$$\tau_{AS} = \frac{\tau_{Ae}}{\tau_{AA}} \tag{2.39}$$

$$r_s = 0.0685 + (1 - B_a) \cdot (1 - \tau_{AS}) \tag{2.40}$$

B_a is called the forward-scattering ratio, the extreme value of B_a are:

$$B_a = \begin{cases} 1\ for\ all\ forward\ scattering \\ 0.5\ for\ isotropic\ scattering \\ 0\ for\ all\ backwardcattering \end{cases}$$

K_1 is a fitted value based on the results of SOLTRAN code.

(Bird and Hulstrom 1981) suggested $B_a = 0.84$ and $K_1 = 0.385$ be used in this model given the location is in urban area. r_g is the surface albedo which is taken the value of 0.2 for Beijing.

Method for Diffuse Horizontal Irradiance (DIF)

The DIF is then derived from GHI and DNI based on their intrinsic relationship (Bird and Hulstrom 1981).

$$GHI = DNI \cdot cos\Theta_Z + DIF \tag{2.41}$$

Therefore,

$$DIF = GHI - DNI \cdot cos\Theta_Z \tag{2.42}$$

2.4 Characterizing the Optical Depth of Aerosols

Aerosol optical depth (AOD) is a measure of the extinction of the solar irradiance due to particles' (dust, smoke, pollution) scattering and absorption effect. In another words, AOD tells how much direct sunlight is prevented from reaching the ground by these aerosol particles. It is a dimensionless number that is related to the amount of aerosol in the vertical column of atmosphere above the observation location.

AOD varies spectrally, therefore, to seek full understanding of the AOD profiles at a given location and time, measurements at multiple wavelengths and shorter time intervals are desired. Modern instrumentations have made wider coverage of AOD at its corresponding wavelength available, at the same time, AOD are measured per couple minutes instead of per day. These progresses are boosted by global wise AOD measurement networks, such as AERONET (AErosol RObotic NETwork; http://aeronet.gsfc.nasa.gov/), the SKYNET branch measurements and and temporally highly resolved modeled data such as MATCH (they represent only climate (averaged) values for a few years, which do not address high-frequency changes.)

Ground-measured AOD data are believed to be the most accurate in term of characterizing the optical depth of aerosols. In general, the so called ground measured AOD data, however, is retrieved from the ground measured DNI.

The CIMEL sunphotometer (Figure 7), for example, is the standard instrument of the AERONET, it measures direct radiation from the sun at wavelengths ranging from 340 nm to 1020 nm and the angular distribution of sky radiance at four wavelengths (440, 675, 870, and 1020 nm).

Figure 7. The Cimel sunphotometer (CSPHOT)

Although AOD at multiple wavelengths are available at locations within the network, not all sites have identical wavelengths coverage, i.e. the typical measured wavelengths at each location varies. This requires a generalization of the different measurements. A practical procedure is given in (Gueymard 2012).

According to the Ångström's Law,

$$k_{\alpha\lambda} = \beta \cdot \left(\frac{\lambda}{\lambda_0}\right)^{-\alpha} \tag{2.43}$$

where $k_{\alpha\lambda}$ is AOD at wavelength λ in nm, and λ_0 is equals to 1000 nm, β is the Ångström turbidity coefficient (or AOD at 1 μm), and α is the wavelength exponent (also know as "Ångström parameter" or "Ångström exponent"). If AOD is know at two wavelengths only, λ_1 and λ_2, α and β can be determined by manipulating Eq. (2.44-45):

$$\alpha = -\ln\left(\frac{k_{\alpha\lambda 1}}{k_{\alpha\lambda 1}}\right) / \ln\left(\frac{\lambda_1}{\lambda_2}\right) \tag{2.44}$$

$$\beta = k_{\alpha\lambda 2} \cdot (\frac{\lambda_2}{\lambda_0})^{\alpha} \tag{2.45}$$

With this procedure, AOD at unknown wavelength could derived from Eq. (2.43)

Another way to characterizing the general optical depth of aerosols is though a broadband turbidity index, such as the Linke turbidity factor, T_L, and the boradband aerosol optical depth (BAOD), k_a, also known as the Unsworth-Monteith coefficient. In this project, these two factors are not necessary, however, detailed calculation procedures can be found in (Gueymard 2012).

The generalized AOD representations are further used to calculate the aerosol transmittance, τ_{Ae}, using Eq. (2.19) in Bird clear sky model.

In comparison, τ_{Ae} is calculated differently at other clear sky formulations, for example, in METSTAT model,

$$\tau_{Ae} = \exp(-m \cdot k_a) \tag{2.46}$$

where m is the air mass, and k_a is the broadband aerosol optical depth.

In the Modefied Iqbal-C Model,

$$\tau_{Ae} = (0.12445 \cdot \alpha - 0.0162) + (1.003 - 0.125 \cdot \alpha) \tag{2.47}$$

$$\times \exp[-m_p \cdot \beta \cdot (1.089 \cdot \alpha + 0.5123)] \tag{2.48}$$

where α is the Ångström exponent and β is the Ångström turbidity coefficient, m_p is pressure-normalized air mass.

2.5 Validation of Clear Sky Model with TMY Weather File

The solar radiation modeling methods mentioned above play a major role in generating new weather files that are derived from the TMY file. We therefore need to validate the modeling methods by testing their capability of regenerating the TMY solar data given the same environmental inputs. Our focus of the solar radiation modeling is on the clear sky models as it contains the AOD model, which is the major interest of this study. The cloud models are intended to be excluded from the study in order to eliminate the effect from cloud.

To validate the clear sky model with the clear sky solar radiation data in the TMY weather file, we first filter out the solar radiation data that are under cloudy sky conditions. In the TMY file, the opaque sky cover (with a value between 0 and 10) represents the "amount (1 tenth) of sky dome cover by clouds or obscuring phenomena that prevent observing the sky or higher cloud layers at the time indicated" (Wilcox and Marion 2008). We delete the solar radiation data when opaque sky cover is not equals to 0, and the remaining data is taken to be the solar radiation data under clear sky conditions. We take the atmospheric pressure, perceptible water, and broadband aerosol optical depth associated with the remaining solar radiation data as the inputs to the clear sky model described in previous section. The model calculates GHI, DNI and DIF with the environmental parameters and the geographical information that matches the TMY file. Figure 8-10 show the comparison of results and TMY file's solar radiation profiles. The regression line show a good correlation exist between the simulated and TMY solar irradiance data. In addition, the slopes of the regression equation are close to 1, indicating the model is adequate in reproducing the measurement data.

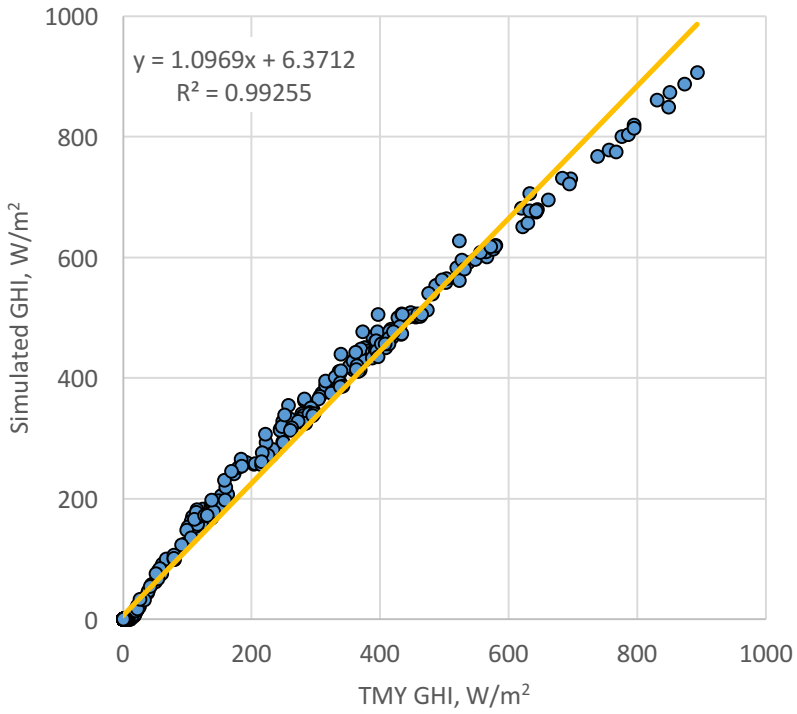

Figure 8. Comparison of simulated vs. TMY global solar irradiance

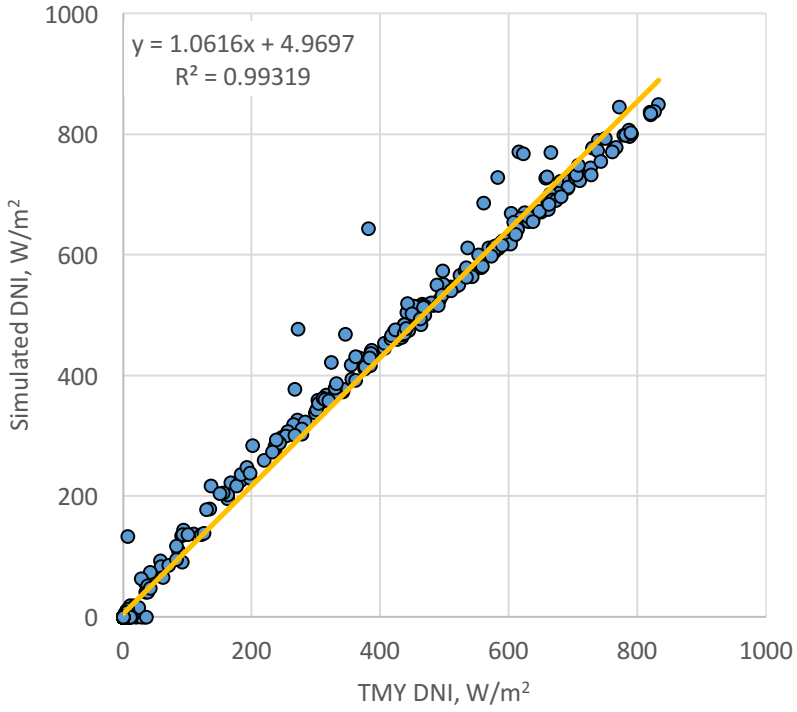

Figure 9. Comparison of simulated vs. TMY direct normal irradiance

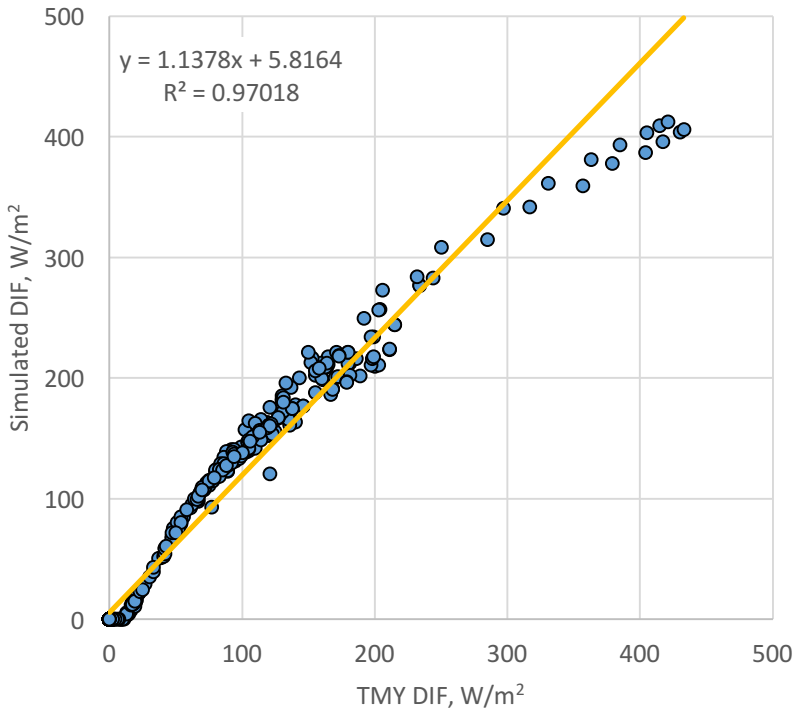

Figure 10. Comparison of simulated vs. TMY diffuse horizontal irradiance (DIF)

CHAPTER 3

SOLAR SHIFT

3.1 Analyzing Current and Historical AOD of Beijing

Beijing has a temperate and continental monsoon climate, with four distinct seasons. Studies have shown that high AOD occurs during March to August, with dust events (in spring) and hot and humid weather (in summer) being the causes. We analyzed the 3240 days of daily average AOD from 2001 to 2015.

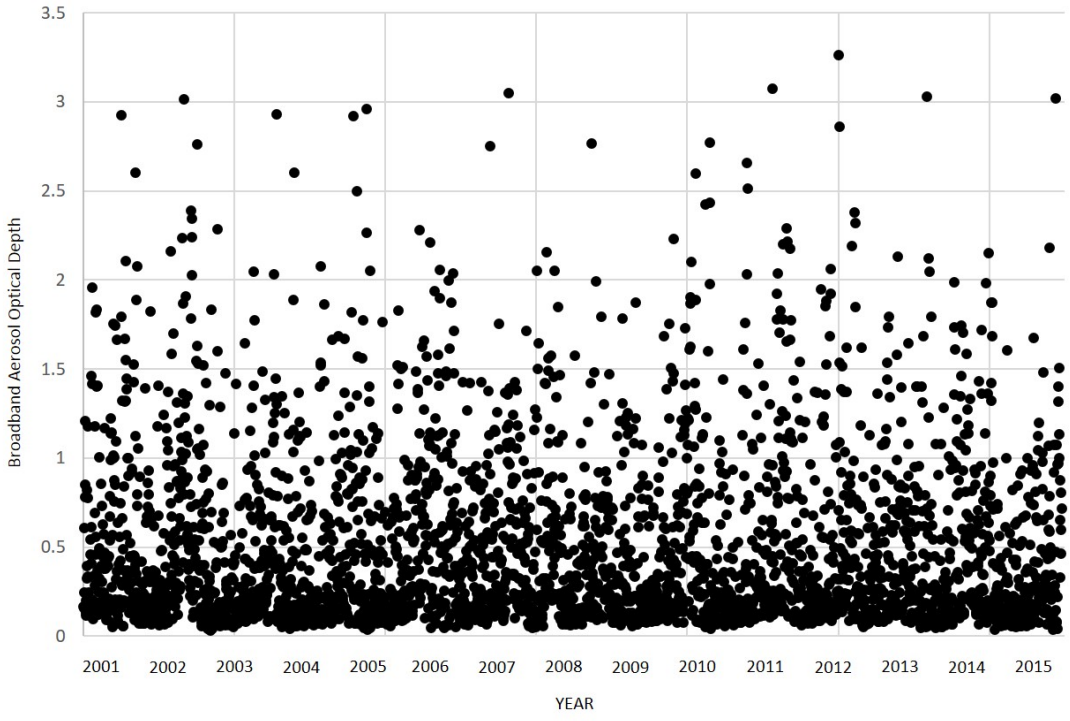

Figure 11. Daily average AOD measured at AERONET site in Beijing from 2001 to 2015

The AOD data for Beijing are acquired from the AERONET website under the Aerosol Optical Depth product category. There are three versions of data sets available for the AOD product, the level 1.0, level 1.5 and level 2.0. The feature of each version is explained below.

- Level 1.0 - unscreened data but may not have final calibration applied
- Level 1.5 - cloud-screened data but may not have final calibration applied. These data are not quality assured.
- Level 2.0 - pre- and post-field calibration applied, cloud-screened, and quality-assured data

We take the level 2.0 AOD data because of its high quality, however, it is noted that there are less data points in the AOD level 2.0 product compared to the lower ranked data products. In order to get a full year AOD data, we need interpolate and extrapolate the missing data points, the procedures are described below.

We first downloaded the level 2.0 daily average AOD data for Beijing on 2013, 2014 and 2015. For the missing daily average data points for a specific year, if the data points at the same day of the year are available from the other two years, we fill in the missing data points with the average of other two years'. Similarly, if the missing data points are only available from one of other years, we fill in the missing data points with whichever year's that is available. For those data points that are missing across all three years, we extrapolate the missing data points with the previous monthly average of that year.

Here we take the AOD data at wavelengths of 440 nm and 675 nm measured at the AERONET Beijing station. We calculate the Ångström turbidity coefficient β and Ångström parameter α from the two bands measurements using Eq. (2.44-45). The AOD at 380 nm and 550 nm are then calculated using Eq. (2.43). Finally, we calculate the broadband aerosol optical depth (BAOD) using Eq. (2.20).

The broadband aerosol optical depth in 2013, 2014 and 2015 are compared to the AOD data recorded at the SWERA TMY file for Beijing. We plot the synthesized 2014 BAOD data from AERONET and the BAOD in the TMY file in the Figure 12 below. It can be observed that the recent measured AOD data have a larger variation compare to the AOD from the TMY file. This indicates the AOD data at the TMY file are not likely representative of recent conditions in Beijing. We tried to confirm on the resources of the AOD recordings in the SWERA TMY file, however as the SWERA project is terminated years ago, the data sources are hardly mentioned at any of the project reports we could find. We could infer from many sources that the solar radiation data (DNI, GHI, DIF) in SWERA TMY files are generated by the NREL's METSTAT model. The hourly AOD data linked to the METSTAT model are simulated through empirical equations according to the geographic location (Gueymard 2012, Sengupta, Habte et al. 2015).

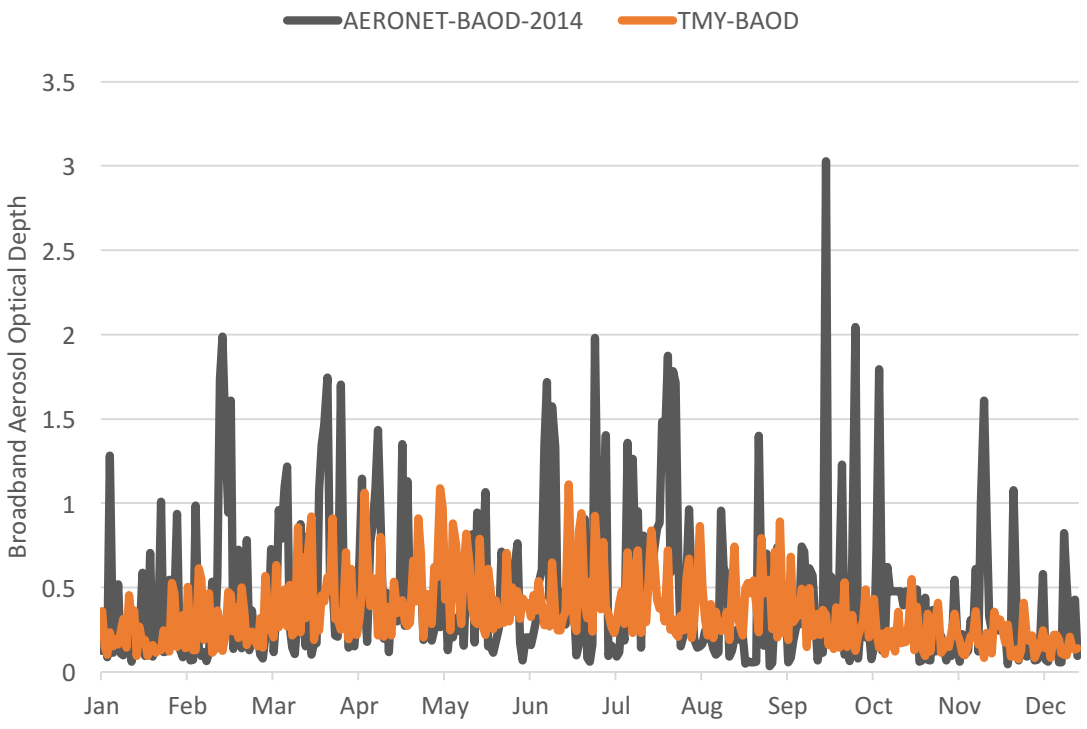

Figure 12. Comparison of the broadband aerosol optical depth in TMY weather file and from AERONET database for Beijing on 2014

3.2 Projection of AOD for Beijing in 2050

In addition to the current status of AOD and the historical data from the TMY, we also project the expected AOD level of Beijing in 2050. The general consensus is that the pollution level in China would decrease as a consequence of the stringent emission regulations and progresses made in renewable and clean energy technologies. However, aerosols in the atmosphere are very closely related to the climate and other metrological phenomenon, the climate change would also play a significant role in predicting the future aerosol concentrations.

(Zhang and Reid 2010) have analyzed the ten-year MODIS (Moderate Resolution Imaging Spectroradiometer) and MISR (Multi-angle Imaging Spectroradiometer) AOD data, both being satellite derived AOD data. Results show a decadal increase of AOD in Eastern China being 0.07-0.1. We take the trend concluded from the past ten-year AOD as our worst scenario, i.e. assume we will not have any form of mitigation in aerosol emissions and the pollution will keep getting worse.

In a different scenario, we are being optimistic about the future aerosol levels and predict the AOD will reduce in consequence. (Jiang, Liao et al. 2013) have investigated the projected 2000–2050 changes in concentrations of aerosols in China, the aerosol projection has relied on the climate and emissions change given by the IPCC A1B scenario. The work concluded that the net reduction of seasonal mean PM2.5 concentrations in eastern China by 1–8 μg m^{-3} (or 10–40 %) over 2000– 2050. As AOD and PM2.5 follows a close to linear relationship, we assume the same reduction in AOD levels in 2050. Based on these AOD trends, we could generate two future AOD profiles with either optimistic or pessimistic projections. The daily AOD profiles of 2014 synthesized in previous section is taken as the base of the modification. The four scenarios of daily AOD profiles are listed as follows. Figure 13 illustrate the different AOD profiles in the month of July.

- Scenario 2050 A: optimistic projection AOD level in 2050, assuming the daily average AOD will drop 30% based on the scenario 2014 AOD profile.
- Scenario 2050 B: pessimistic projection AOD level in 2050, assuming the daily average AOD will increase at the rate of 0.1/decade based on the scenario 2014 AOD profile.
- Scenario 2014: Synthesized AOD profile based on the 2013 -2015 AERONET AOD level 2.0 product, with 2014 AOD data being the bone and 2013, 2015 data being the supplementary for the missing data points.
- Scenario TMY: daily AOD in the SWERA TMY file.

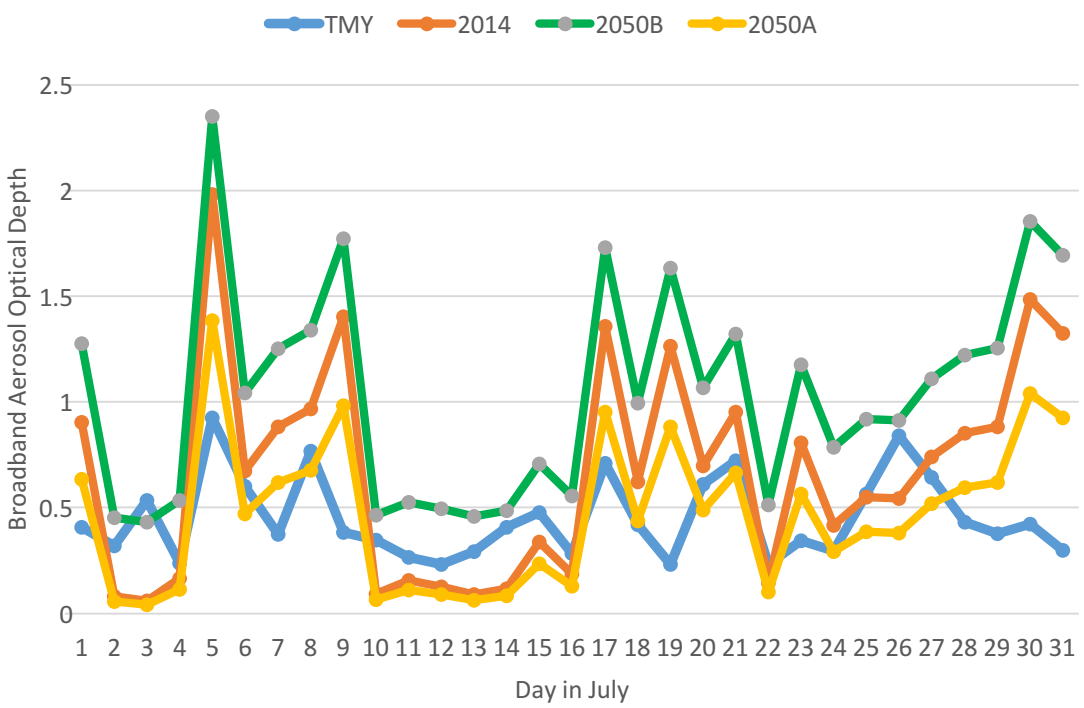

Figure 13. Comparison of daily aggregated broadband optical depth for the 4 scenarios during a summer month

3.3 Creation of New Weather Files

In order to perform building energy simulation, a complete weather file is needed. The clear sky models described in Chapter 2 provide methods to calculate clear sky solar irradiances given AOD as a major input, however, these solar data cannot be directly used in the building energy simulation due to the cloud information being unknown. In this project, we are focused on the AOD variations and its impact on building energy consumptions, therefore, we want to control other variants to be constant.

Figure 14-15 illustrate the procedures generating new DNI and GHI for different scenarios. For scenarios DNI, we first calculate TMY aerosol transmittance ($\tau_{Ae,TMY}$) using Eq. (2.19) given the TMY AOD data as input. We then take the DNI data from the TMY file and divided by $\tau_{Ae,TMY}$, the remaining portion is then multiplied by the scenarios aerosol transmittance ($\tau_{Ae,Scenarios}$) to get the scenario cloudy DNI, these procedures are shown in Eq. (3.1).

$$DNI_{Scenarios} = DNI_{TMY} \cdot \frac{\tau_{Ae,Scenarios}}{\tau_{Ae,TMY}} \tag{3.1}$$

The scenario GHI are calculated in a slightly different way, and this is because that the calculation of cloudy GHI in Eq. (2.25) is in a different form with the DNI calculation in Eq. (2.12). We first calculate the TMY clear sky GHI using the Bird clear sky model (Eq. (2.35)), the perceptible water information is also taken from the TMY file and linked to the Bird model. Next, we calculate the cloud modifier, ktm from TMY clear sky GHI and cloudy GHI using Eq. (2.25), here we further simplify this equation such that,

$$ktm = \frac{GHI}{Ghc} \tag{3.2}$$

Lastly, the scenario DIF is calculated based on the intrinsic relationship between GHI, DNI and DIF using Eq. (2.41).

The above mentioned procedures are performed for a whole year (8760 hours) for each scenario, we then replace the GHI DNI and DIF in the TMY file with the calculated

scenarios solar irradiance data to generate new sets of weather files. The procedures of calculating DNI and GHI are illustrated in figure 14-15.

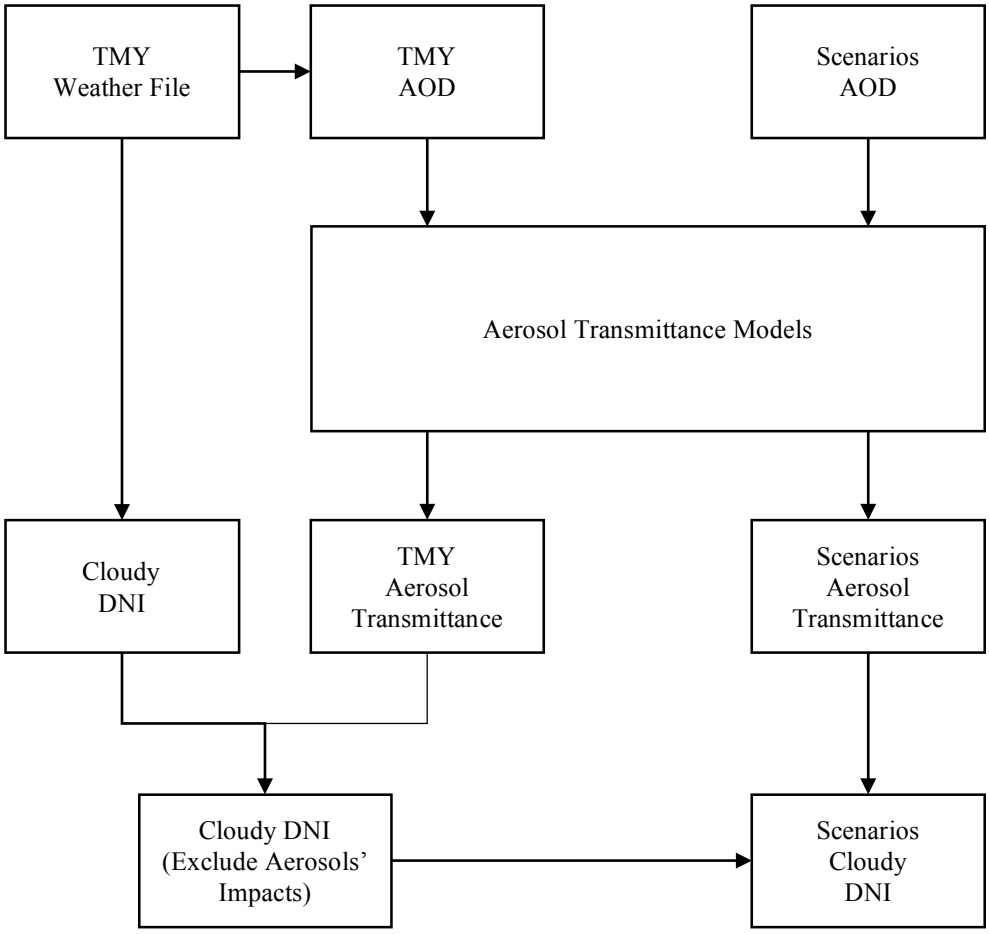

Figure 14. Procedures of generating DNI

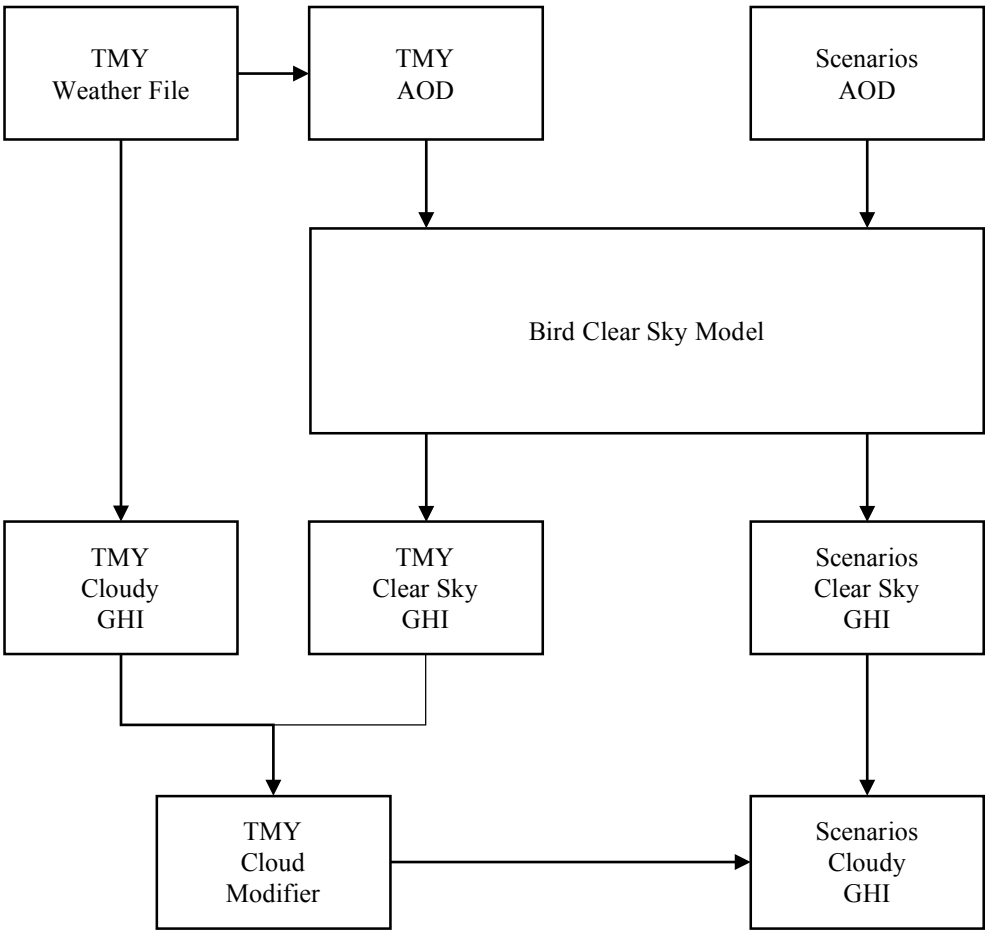

Figure 15. Procedure of generating GHI

Figure 16-18 plot the monthly aggregated GHI, DNI and DIF for the TMY and each scenario. Table 2-4 listed the annual total GHI, DNI and DIF for the four scenarios.

It is clear that the variation in aerosols emissions has caused effects on the simulated solar irradiances. For the annual total global horizontal irradiance (GHI), the 2014 scenario shows a reduction of 1.7 %, the 2050A scenario shows an increase of 2.5 % and 2050B shows a reduction of 7.6 %, in comparison to the TMY scenario; For the annual total direct normal irradiance (DNI), the 2014 scenario shows a reduction of 13.3 %, the 2050A scenario shows an increase of 10.5 % and 2050B shows a reduction of 49.4 %, in comparison to the TMY scenario; For the annual total diffuse horizontal irradiance (DIF), the 2014 scenario shows an increase of 7.3 %, the 2050A scenario shows a reduction of 3.5 % and 2050B shows an increase of 23.5 %, in comparison to the TMY scenario. The solar shifting effect can be observed from these variations. When the haze pollution is severe, part of the direct normal irradiance is absorbed and truncated, and other part is scattered and added to the diffuse horizontal irradiance. When the haze pollution is getting better, an opposite trend is observed. The hypothesis 1 is proved to be true based on these findings.

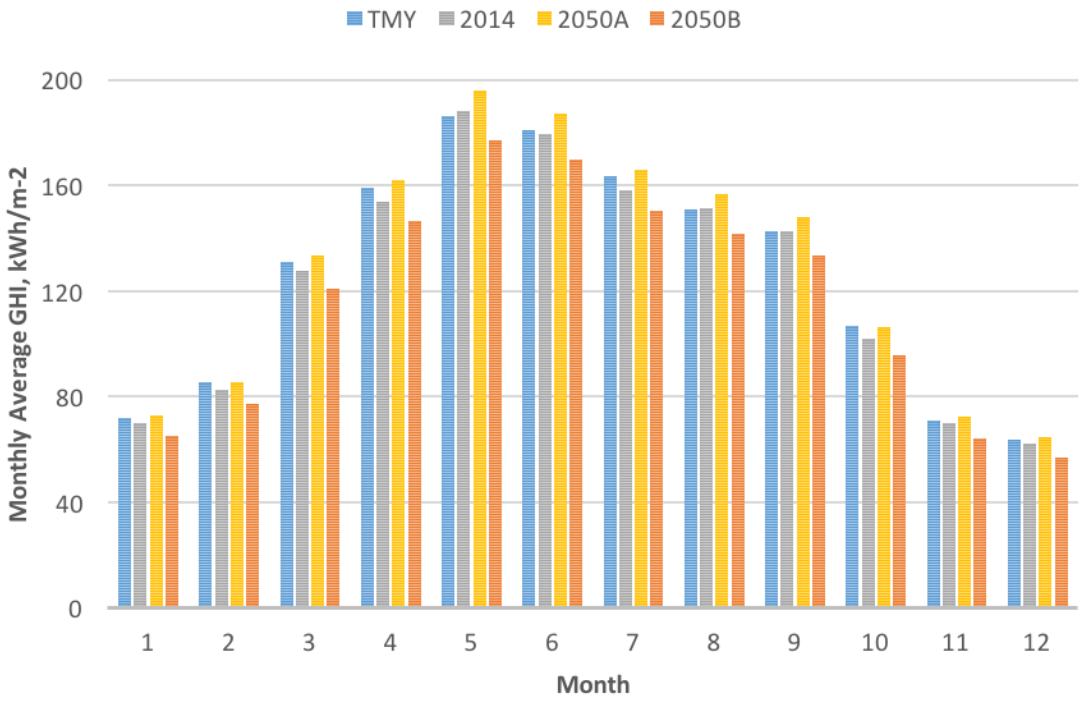

Figure 16. Monthly aggregated global horizontal irradiance (GHI)

Table 2. Annual Total GHI for the 4 scenarios

Scenarios	**TMY**	**2014**	**2050A**	**2050B**
Annual Total GHI (kWh/m-2)	1513	1487	1551	1399
Percent Increase based on the TMY Level	0 %	-1.7 %	2.5 %	-7.6 %

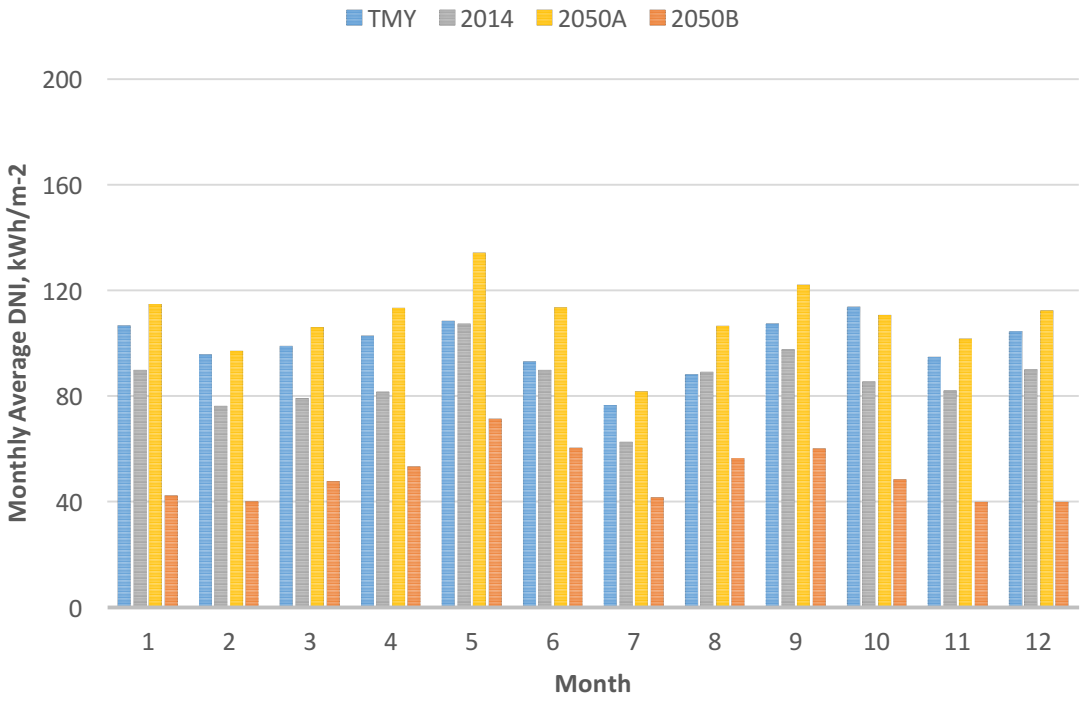

Figure 17. Monthly aggregated direct normal irradiance (DNI)

Table 3. Annual Total DNI for the 4 scenarios

Scenarios	**TMY**	**2014**	**2050A**	**2050B**
Annual Total DNI (kWh/m-2)	1189	1031	1314	601
Percent Increase based on the TMY Level	0 %	-13.3 %	10.5 %	-49.4 %

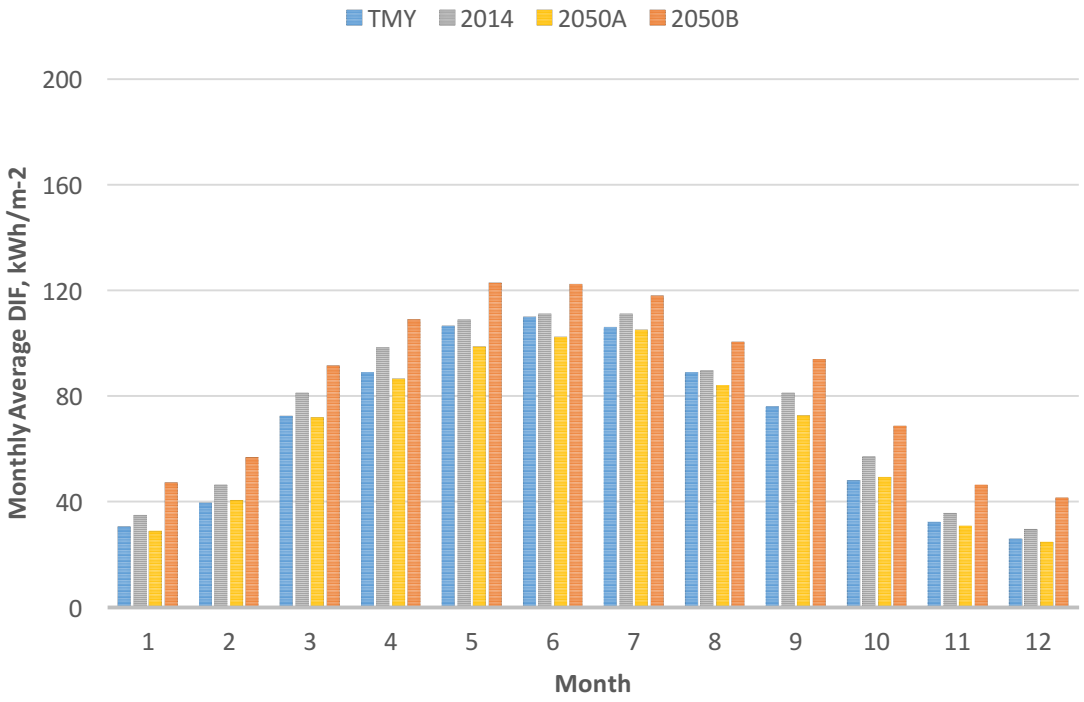

Figure 18. Monthly aggregated diffuse horizontal irradiance (DIF)

Table 4. Annual Total DIF for the 4 scenarios

Scenarios	**TMY**	**2014**	**2050A**	**2050B**
Annual Total DIF (kWh/m-2)	825	885	796	1019
Percent Increase based on the TMY Level	0 %	7.3 %	-3.5 %	23.5 %

CHAPTER 4

IMPACTS ON BUILDING ENERGY PERFORMANCE

4.1 Case Study Building Model

We take the Chinese reference building model created by Peng Xu's group at Tongji University of China as our case study building model. The reference building is a 5-floor medium office building with gross floor area of 3800 m^2 and floor height of 3.6 m. Floor plan is illustrated in figure 20. Each floor has two separated zones with identical internal load density: lighting density is 8 W/m^2, appliances density is 8 W/m^2 and people 4 m^2/Person. The window-to-wall ratio is 36% and the building shape coefficient is 0.17. The U factor for exterior wall, roof and windows are 0.567 W/ (m^2·K), 0.569 W/ (m^2·K) and 2.67 W/ (m^2·K), respectively. The window SHGC is 0.821 and visible light transmittance is 0.812. Cooling are supplied by fan coil units in summer and heating is supplied through district heating and radiators. During occupied hours, the thermostat is set to 24 °C in summer and 22 °C in winter. During unoccupied hours, set points are 40 °C and 13 °C for summer and winter separately. A constant relative humidity of 50% is maintained in both summer and winter. The cooling supply air temperature is 16 °C and 32 °C for heating. Cold and hot supply water temperatures are 7 °C and 90 °C respectively. The water pump and fan both have a constant mass/air flow rate. All equipment are sized based on the design day method based on the weather file. Table 5 listed detailed building and system parameters.

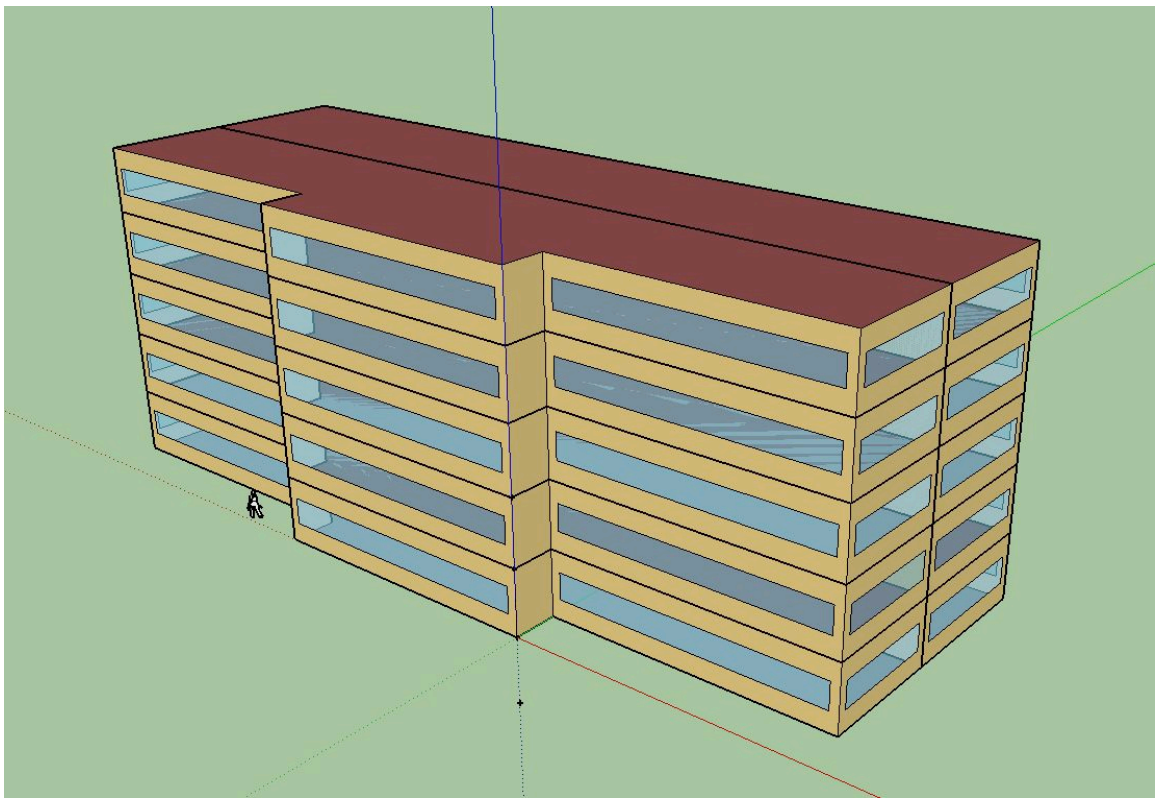

Figure 19. 3D model of the case study medium office building

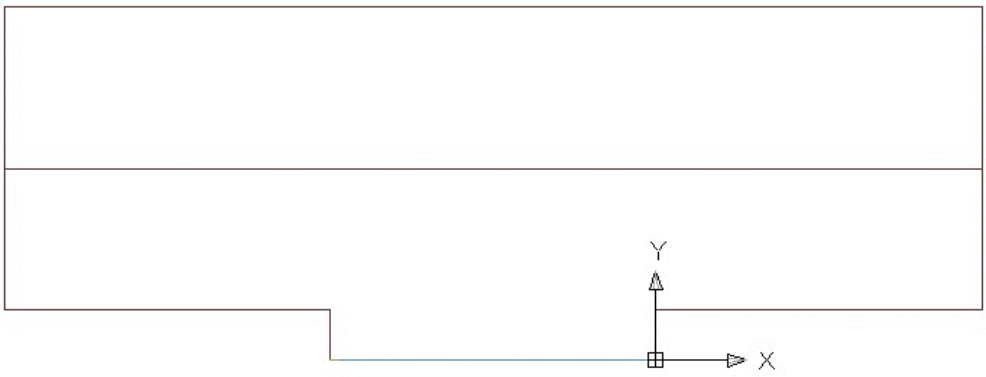

Figure 20. Thermal zone division for each floor

Table 5. General description of the case study building

Building General	
Building Location	Beijing
Source Energy	Electricity, Natural Gas
Building Type	Office
Gross Area	3800 m^2
Building shape coefficient	0.17
Number of Floors	5
Window-to-wall Ratio	36 %
Orientation	South
Space Type	Office
Floor Height	3.6 m
Building Envelopes	
Exterior Wall	
U factor	0.567 W/(m^2·K)
Roof	
U factor	0.569 W/(m^2·K)
Window	
U factor	2.67 W/(m^2·K)
SHGC	0.821
Visible Light Transmittance	0.812
HVAC Systems	
System Type	
Cooling	Fan Coil Unit
Heating	District Heating + Radiator
System Capacity	
Cooling Capacity	Design Day
Heating Capacity	Design Day
System Efficiency	
	＞2.6
System Parameters	
Occupied Thermostat Settings	Summer 24 °C /Winter 22 °C
Unoccupied Thermostat Settings	Summer 40 °C /Winter 13 °C
Relative Humidity	Summer 50 %/Winter 50 %
Supply Air Temperature	Summer 16 °C /Winter 32 °C
Cold Supply Water Temperature	7 °C
Hot Supply Water Temperature	90 °C
Water Pump	Constant Mass Flow Rate
Fan	Constant Air Flow Rate
Internal Loads	
Lighting Density	8 W/m^2
Appliance Density	12 W/m^2
Occupancy	4 m^2/Person

4.2 Building Energy Analysis

To further study the building's response to the AOD variation, we performed dynamic building simulation using EnergyPlus to evaluate the hourly energy consumption of the reference building. The weather files generated based on the four AOD scenarios serve as the boundary conditions of the building model.

Table 6 lists the annual Energy Use Intensity (EUI) breakdown for each weather scenario. Figure 21 illustrates the comparison of EUI of different scenarios.

Figure 22-23 show the cooling (HVAC) energy consumption and the heating (district heating) energy consumption of the reference building under different scenarios of projected climatic conditions.

Table 6. Annual EUI breakdowns for the 4 scenarios

EUI (kWh/m^2)	TMY	2014	2050A	2050B
Heating (District Heating)	23.65	24.88	23.30	28.32
Cooling	18.94	18.95	19.14	18.66
Interior Lighting	16.18	16.18	16.18	16.18
Interior Equipment	18.80	18.80	18.80	18.80
Fans	3.51	3.51	3.51	3.50
Pumps	0.71	0.71	0.71	0.71

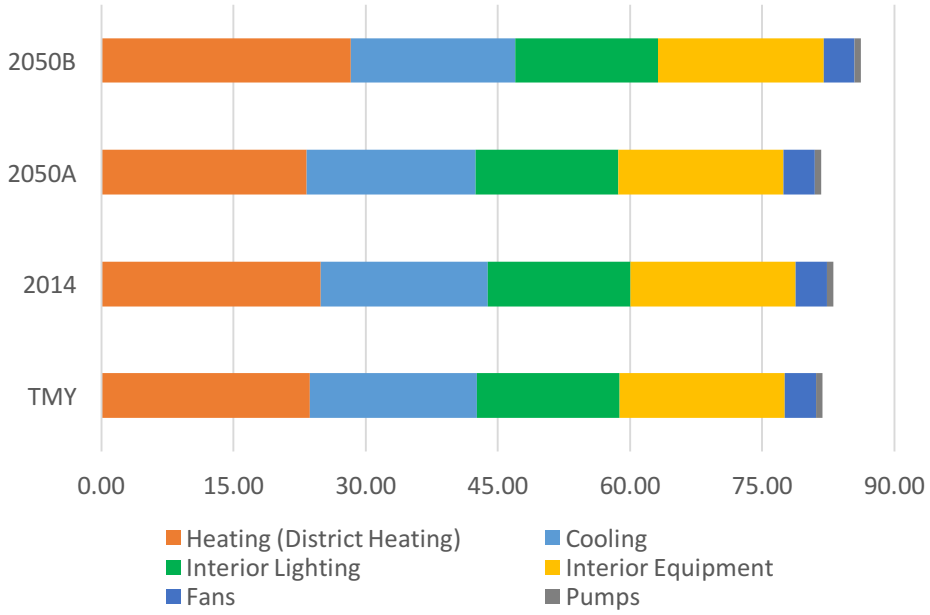

Figure 21. Annual EUI for the 4 scenarios

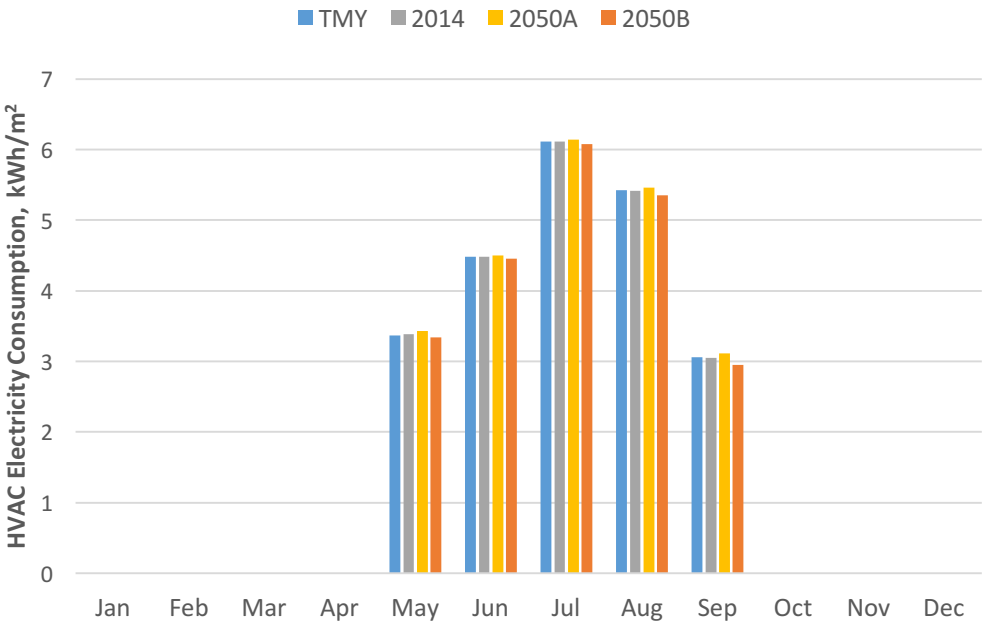

Figure 22. HVAC electricity consumption for the four scenarios

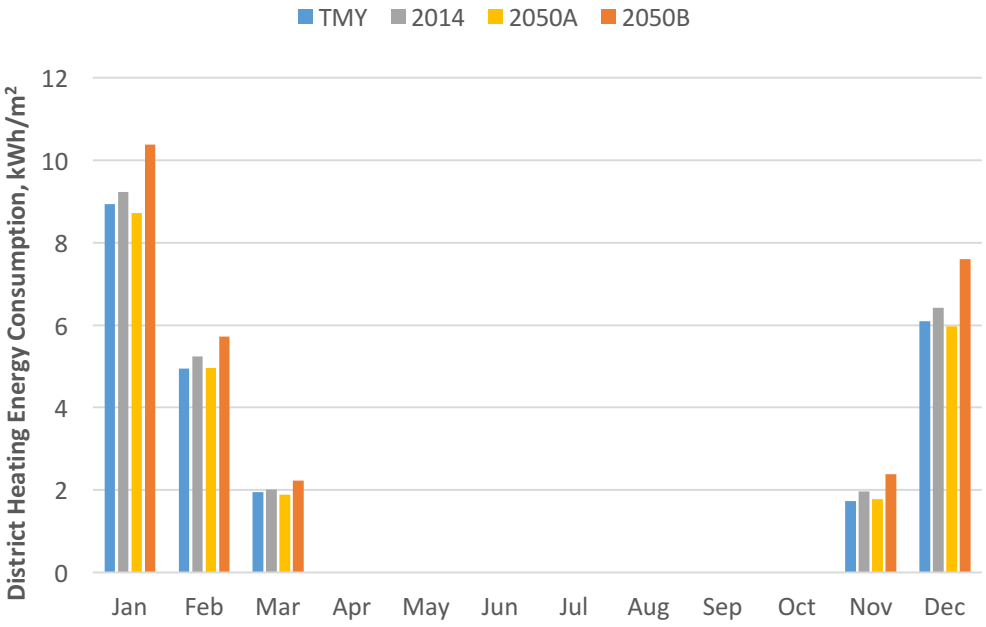

Figure 23. District heating energy consumption for the four scenarios

From EUI breakdowns shows in Table 6, we see apparent alternations in district heating energy among the four scenarios, whereas less variations in cooling energy consumption.

The optimistic scenario (2050A) shows a reduction of 1.5 % in (district) heating energy. We could interpret these outcomes through intuition that when the haze pollution is severe, less solar energy could penetrate the aerosol particles and finally pose on the building envelope, therefore in winter the “free heating” opportunity is reduced, and more heating energy is needed. In summer, the heavy aerosols in a severe scenario help block the heat from the solar and keep the building cool where less cooling energy are demanded.

The less variations observed in cooling energy compared to heating energy among the four scenarios could be attributed to the nature of cooling and heating equipment (i.e. the cooling COP is higher than the efficiency of district heating).

Hypothesis 2 is proved to be true according to the above findings.

4.3 Heating Load Analysis and Implications on System Sizing

Heating loads of the reference building are further evaluated under each climatic scenario. Figure 25 shows the cumulative probability of scenario heating loads. The value of building heating load at the 0.996^{th} quantile of the CDF is used for system sizing (Sun, Gu et al. 2014), which means if we size the heating energy system based on this value, the heating demand could be met at 99.6% of the total hours of the simulation period. This value would be interesting for us to further investigate how aerosol emission variation would impact the district heating system capacity in meeting the heating demand. Figure 24 shows the 99.6 percentile of cumulative heating load for each scenario, the 0.996^{th} quantile of the CDF for TMY, 2014, 2050A and 2050B are 298.2 kW, 305.8 kW, 300.6 kW, and 314.3 kW. The same value calculated based ASHRAE design day is 381.9 kW. This implies the current system sizing based on ASHREA design day method could meet the heating demands under all possible scenarios evaluated in this study, hypothesis 3 is therefore rejected from this conclusion. However, it also indicates there are huge potential waste of capacity in current design day method.

Table 7. Critical heating load for each scenario

Scenarios	**TMY**	**2014**	**2050A**	**2050B**	**ASHREA Design Day**
Critical Heating Load for Sizing (kW)	298.2	305.8	300.6	314.3	381.9
Comparisons to scenario TMY (%)		+ 2.55 %	+ 0.80 %	+ 5.40 %	28.07 %

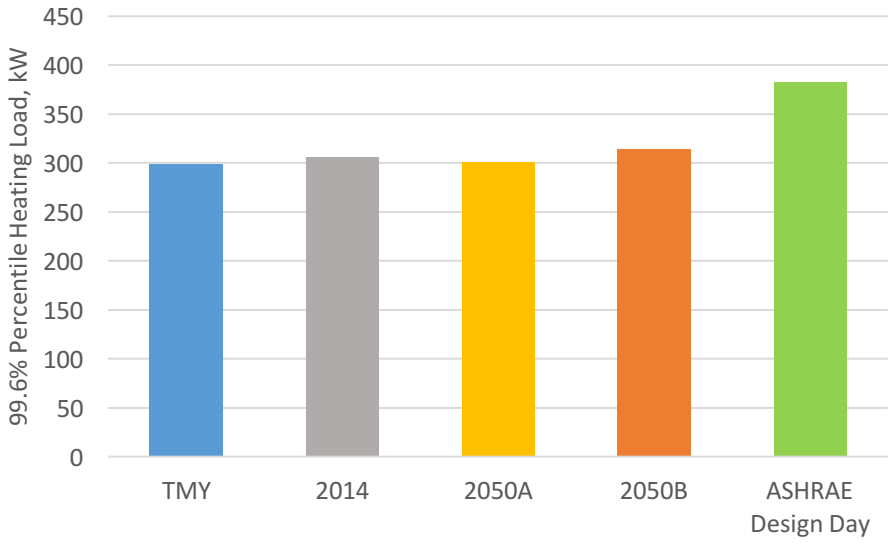

Figure 24. Heating loads at the 0.996th quantile of the CDF for the four scenarios

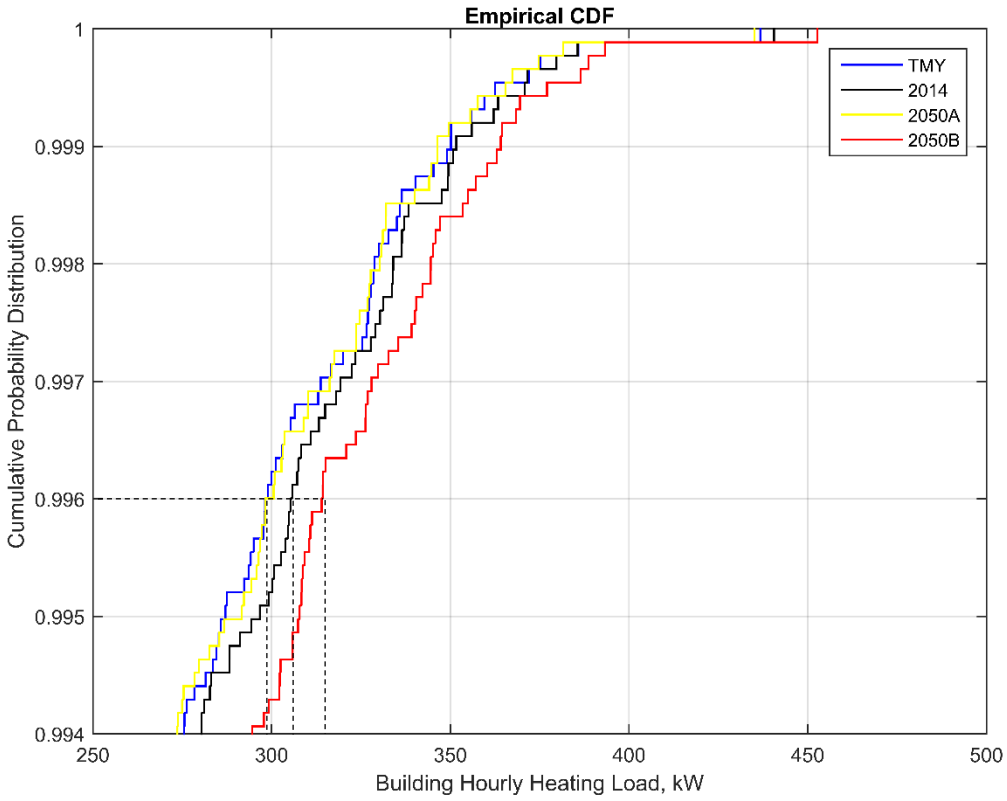

Figure 25. Cumulative probability distribution of building hourly heating load for the four scenarios

CHAPTER 5

CONSCLUSION AND FUTURE WORK

5.1 Conclusion Remarks

The following conclusions result from this study:

1. AOD has an apparent impact on the modeled solar irradiance data (GHI, DNI, DIF) which are potentially used in accessing building energy performance. By replacing the AOD in current TMY weather file with three different AOD profiles, the AERONET measurements on 2014, the optimistic and the pessimistic projections in 2050, the variation of solar irradiance has been observed. The results show that the increase of AOD levels will have a small negative impact on GHI, a larger negative impact on DNI, and a positive impact on DIF. These observations align well with findings from similar studies.
2. The AOD profile used in the current TMY weather file from the SWERA project is unrepresentative and underestimates the AOD levels if compare to the recently measured data for 2014. This leads to a redistribution of a part of the direct solar irradiance that is either absorbed or scattered, and thereby increases diffuse solar irradiance. From our study the building district heating energy consumption increases by 5 % due to this shift.
3. The variation of solar irradiance due to the current and future projections of AOD shows apparent impacts on building energy consumptions, with small impacts on cooling electricity consumption and large impact on (district) heating energy consumption. Under a pessimistic prediction of the AOD levels in 2050, where we assume the current pace in aerosol emissions to be constant, the monthly average heating energy consumption could increase 10 % compared to the TMY scenario.

4. The 99.6th percentile heating load for all scenarios are found to be below the critical heating load generated by the ASHRAE design day method. This indicate the current sizing method is safe enough considering all possible aerosol emission scenarios that are restrained in this study. However, the 2014 and 2050B scenarios have show increases in the critical heating load by 2.6 % and 5.4 %, respectively, comparing to the TMY scenario.

5.2 Future Work

The future work should target:

1. Evaluation of other effects of haze pollution on building outcomes, such as daylighting, natural ventilation potentials, HVAC system efficiency, occupants activity, appliances etc.
2. Current study does not consider the correlation between AOD and other environmental variables (dry bulb temperature, wet bulb temperature, relative humidity etc.). In reality, the aerosol levels could have a direct or indirect impacts on the atmosphere and the surrounding environment. In the future, one needs to quantify these correlation effects and modify all impacted environmental variables in new weather files.
3. The uncertainties in the modeling procedures and the measurement data are not well discussed in this study. Future work in this direction should include literature review on the solar radiation model uncertainties and AOD measurement uncertainties. The model form uncertainties introduced in calculating the aerosol transmittance can be represented in utilizing different aerosol transmittance algorithms in conjunction with measurements.
4. Re-evaluate the future building energy consumption considering both aerosols emissions and climate change.

5. This study only evaluates the building performance for one type of buildings (office building) and one Chinese city (Beijing). The future work should include more Chinese cities as well as building types.

REFERENCES

(2006). "User Manual for SWERA: Designing Renewable Resource Assessment Projects and Using Assessment Products."

Barnaby, C. S. and D. B. Crawley (2011). "Weather data for building performance simulation." Building Performance Simulation for Design and Operation: 37-55.

Bellouin, N., et al. (2005). "Global estimate of aerosol direct radiative forcing from satellite measurements." Nature **438**(7071): 1138-1141.

China pollution: First ever red alert in effect in Beijing. (2015) In BBC News China. Retrieved April 18, 2016, from http://www.bbc.com/news/world-asia-china-35026363

Bird, R. E. and R. L. Hulstrom (1981). Simplified clear sky model for direct and diffuse insolation on horizontal surfaces, Solar Energy Research Inst., Golden, CO (USA).

Chameides, W. L., et al. (1999). "Case study of the effects of atmospheric aerosols and regional haze on agriculture: An opportunity to enhance crop yields in China through emission controls?" Proceedings of the National Academy of Sciences **96**(24): 13626-13633.

Chen, Z., et al. (2013). "China tackles the health effects of air pollution." The Lancet **382**(9909): 1959-1960.

Crawley, D. B., et al. (2001). "EnergyPlus: creating a new-generation building energy simulation program." Energy and Buildings **33**(4): 319-331.

Fu, Q., et al. (2008). "Mechanism of formation of the heaviest pollution episode ever recorded in the Yangtze River Delta, China." Atmospheric Environment **42**(9): 2023-2036.

Gueymard, C. A. (2012). "Clear-sky irradiance predictions for solar resource mapping and large-scale applications: Improved validation methodology and detailed performance analysis of 18 broadband radiative models." Solar Energy **86**(8): 2145-2169.

Hirsch, J. J. (2006). "eQuest, The QUick Energy Simulation Tool." DOE2. com.

Hong, T., et al. (2014). Building energy benchmarking between the united states and china: methods and challenges. Proceedings of the 8th International Symposium on Heating, Ventilation and Air Conditioning, Springer.

Huang, R.-J., et al. (2014). "High secondary aerosol contribution to particulate pollution during haze events in China." Nature **514**(7521): 218-222.

Ineichen, P. (2008). "A broadband simplified version of the Solis clear sky model." Solar Energy **82**(8): 758-762.

Jiang, H., et al. (2013). "Projected effect of 2000-2050 changes in climate and emissions on aerosol levels in China and associated transboundary transport." Atmospheric Chemistry and Physics **13**(16): 7937-7960.

Kan, H., et al. (2012). "Ambient air pollution, climate change, and population health in China." Environment international **42**: 10-19.

Laboratory, U. o. W.-.-M. S. E. and S. A. Klein (1979). TRNSYS, a transient system simulation program, Solar Energy Laborataory, University of Wisconsin--Madison.

Lefevre, M., et al. (2013). "McClear: a new model estimating downwelling solar radiation at ground level in clear-sky conditions." Atmospheric Measurement Techniques **6**: 2403-2418.

Liu, J., et al. (2007). "Significant aerosol direct radiative effects during a pollution episode in northern China." Geophysical Research Letters **34**(23).

Liu, X., et al. (2013). "Formation and evolution mechanism of regional haze: a case study in the megacity Beijing, China." Atmos. Chem. Phys **13**(9): 4501-4514.

Perez, R., et al. (2002). "A new operational model for satellite-derived irradiances: description and validation." Solar Energy **73**(5): 307-317.

Perez, R., et al. (2002). A New Operational Satellite-to-Irradiance Model--Description and Validation. PROCEEDINGS OF THE SOLAR CONFERENCE, AMERICAN SOLAR ENERGY SOCIETY; AMERICAN INSTITUTE OF ARCHITECTS.

Reinhart, C. F. and C. C. Davila (2016). "Urban building energy modeling–A review of a nascent field." Building and Environment **97**: 196-202.

Sengupta, M. and P. Gotseff (2013). Evaluation of Clear Sky Models for Satellite-based Irradiance Estimates, National Renewable Energy Laboratory (NREL), Golden, CO.

Sengupta, M., et al. (2015). Best practices handbook for the collection and use of solar resource data for solar energy applications, National Renewable Energy Laboratory.

Stier, P., et al. (2007). "Aerosol absorption and radiative forcing." Atmospheric Chemistry and Physics **7**(19): 5237-5261.

Sun, Y., et al. (2014). "Exploring HVAC system sizing under uncertainty." Energy and Buildings **81**: 243-252.

Wang, X., et al. (2012). "The secondary formation of inorganic aerosols in the droplet mode through heterogeneous aqueous reactions under haze conditions." Atmospheric Environment **63**: 68-76.

Wilcox, S. and W. Marion (2008). Users manual for TMY3 data sets, National Renewable Energy Laboratory Golden, CO.

Yang, Y., et al. (2015). "Formation mechanism of continuous extreme haze episodes in the megacity Beijing, China, in January 2013." Atmospheric Research **155**: 192-203.

Zhang, J. and J. Reid (2010). "A decadal regional and global trend analysis of the aerosol optical depth using a data-assimilation grade over-water MODIS and Level 2 MISR aerosol products." Atmospheric Chemistry and Physics **10**(22): 10949-10963.